


 Cite this: *Lab Chip*, 2021, 21, 1217

Review of microfluidic approaches for fabricating intelligent fiber devices: importance of shape characteristics

 Ronghui Wu ^a and Taesung Kim ^{*ab}

Shape characteristics, which include the physical dimensions (scale), apparent morphology, surface features, and structure, are essential factors of fibrous materials and determine many of their properties. Microfluidic technologies have recently been proposed as an approach for producing one-dimensional (1D) fibers with controllable shape characteristics and particle alignment, which impart specific functionality to the fiber. Moreover, superfine 1D fibers with a high surface area and ordered structure have many potential applications as they can be directly braided or woven into textiles, clothes, and tissues with two- or three-dimensional (2D or 3D) structures. Previous reviews of microfluidic spinning have not focus on the importance of the shape characteristic on fiber performance and their use in intelligent fiber design. Here, the latest achievements in microfluidic approaches for fiber-device fabrication are reviewed considering the underlying preparation principles, shape characteristics, and functionalization of the fibers. Additionally, intelligent fiber devices with shapes tailored by microfluidic approaches are discussed, including 1D sensors and actuators, luminous fibers, and devices for encoding, energy harvesting, water collection, and tissue engineering applications. Finally, recent progress, challenges, and future perspectives of the microfluidic approaches for fiber device fabrication are discussed.

 Received 1st December 2020,
 Accepted 24th February 2021

DOI: 10.1039/d0lc01208d

rsc.li/loc

^a Department of Mechanical Engineering, Ulsan National Institute of Science and Technology (UNIST), 50 UNIST-gil, Ulsan 44919, Republic of Korea.
 E-mail: tskim@unist.ac.kr

^b Department of Biomedical Engineering, Ulsan National Institute of Science and Technology (UNIST), 50 UNIST-gil, Ulsan 44919, Republic of Korea

1. Introduction

The term “fiber” usually refers to a flexible material with an aspect ratio of more than 10^3 and a diameter of micrometres


Ronghui Wu

Dr. Ronghui Wu received her Ph.D. degree from the College of Textiles, Donghua University (DHU) in 2020. During her Ph. D. period, she worked as a joint training student in the Institute of Biomimetic and Soft Matter, Xiamen University (XMU) for two years. After, she worked as a visiting scholar in the Department of Science, National University of Singapore (NUS) for biomimic spinning in 2018. She is now a postdoc in the

Department of Mechanical Engineering, Ulsan National Institute of Science and Technology (UNIST). Her research interests focus on wearable electronics, regenerated silk fibers, and microfluidic spinning technology for intelligent fiber devices.


Taesung Kim

Prof. Taesung Kim obtained his B. S. and M.S. degree from Seoul National University in 1997 and 1999, respectively, and received his Ph.D. degree from the University of Michigan in 2006, all from the Department of Mechanical Engineering. After being a research fellow at the University of California at Berkeley and Lawrence Berkeley National Laboratory (LBNL, JBEI), he started his independent research career as an assistant professor in

2009 and was promoted to an associate and full professor in 2012 and 2017, respectively, at the Ulsan National Institute of Science and Technology (UNIST). His research interests include micro-/nanofluidics, unconventional microfabrication for mixed-scale micro-/nanofluidic devices and functional nanopatterns, multiphysical transport phenomena at nanoscales, and microfluidic spinning technologies for wearable electronic devices.

or nanometres.²³ 1D fibers are the basic unit of yarn or fabric, and they can be braided or woven into two- or three-dimensional (2D or 3D) materials, such as textiles, braided composites, and biological tissues. Intelligent fiber devices are a critical component of electronic textiles (E-textiles), shape memory fabrics, protective fabrics and other smart textiles.^{25–27} To date, many spinning methods have been developed to fabricate fibers, such as electrospinning,^{25,30–32} wet spinning,^{33–36} melt spinning,⁴² dry spinning,^{43,44} and draw spinning.⁵⁴ However, these spinning technologies involve complicated processes, which can have unpredictable effects on the molecular structure of the spinning solution, and restrict its use to specific material types. Moreover, the fiber scale and morphology are difficult to control using traditional spinning methods (Table 1). To overcome this, microfluidic approaches have been employed to produce fibers appropriate for 1D intelligent devices, which showed significant potential as novel tools for generating micro/nanoscale structures. For example, micro/nanoscale materials were produced by microfluidic approaches with a variety of shape characteristics,⁵⁹ including particles,^{60,61} fibers,^{36,51,62–65} and tubes,⁵⁷ without the use of complicated facilities or devices, where the produced structures were appropriate for use as bottom-up scaffolds and flexible devices.^{71–73} Microfluidics is a discipline that manipulates or processes small amounts of fluids, using micro/nanoscale channel structures with dimensions of microns.^{74–76} Therefore, it can offer many advantages for fiber-based device fabrication, such as the use of small volumes of the material, low production cost, simple apparatus and equipment, short reaction time for producing fiber composites, and high yields.

The shape characteristics, as the basic attributes of the fiber material,²³ include four main factors: the physical dimensions (scale), morphology, surface features, and structure. The performance of fiber devices is highly dependent on controlling the fiber shape characteristics. Microfluidic spinning methods apply mild operating conditions and can be used to produce micro/nanoscale fibers with controllable morphologies, diverse structures, and specific functionality by taking advantage of the precise multi-laminar flows and manipulating the state of each flow in the microchannels.⁶ The laminar flows in the microfluidic channels are generally determined by the fluid viscosity and surface tension, fluidic gravity, and inertia. Therefore, by

appropriately adjusting these parameters, it is easy to control the operating conditions to produce fibers with different shape characteristics, such as hollow,⁵⁷ necklace,⁷⁷ and helical.^{39,78,79} By manipulating the shape characteristics of the fibers produced by microfluidic spinning, diverse wearable fiber devices with water collection, luminous, encoding, and biochemical applications have been obtained (Fig. 1). Therefore, microfluidics provides a potential platform for the fabrication of micro/nanoscale fibrous materials with tuneable shapes for various applications.

Here, we summarize the recent advances in the progress of fiber devices fabricated by microfluidic approaches. First, the critical shape characteristics of the fiber materials fabricated by microfluidic approaches are discussed considering their effect on fiber devices. Additionally, we highlight the microfluidic fabrication methods and performance of intelligent fiber devices for water collection, encoding, sensors, actuators, energy, and biomedical applications. Finally, we discuss recent progress, challenges, and future perspectives of the microfluidic approaches for fiber device fabrication and their prospects for improving the performance of wearable devices.

2. Microfluidic spinning systems for fiber formation

2.1 Microfluidic chips for fiber formation

The design of the fiber spinning system and control of its primary parameters determine the fiber shape characteristics and the subsequent performance of the fiber device. Hence, the microfluidic chip is one of the most important parts of the microfluidic spinning system. Various spinning chips based on cylindrical or rectangular polydimethylsiloxane (PDMS) microchannels, glass micropipettes, metal needles, or tubes have been developed. The chip designs are classified according to the chip morphology: round-capillary chips and patterned plane chips.

In round-capillary chips, the spinning solutions flow through various round capillaries,^{6,18,80–83} facilitating the adjustment of the flow parameters during coaxial flow creation. Such systems have several advantages. First, the round capillaries form perfect cylindrical channels that effectively control the phase behaviour during coaxial flow generation.⁶² In addition, round capillaries are commercially

Table 1 Comparison of different spinning methods

Features	Electrospinning	Dry spinning	Wet spinning	Melt spinning	Microfluidic spinning
Mechanism	Electrostatic driving force	Heat medium	Coagulation bath for solidification	Polymer melting	Coaxial laminar flow
Fabrication condition	Dry	Dry	Wet, relatively mild	Melt, high temperature	Wet, mild
Fiber diameter	Nanometres to few microns	Microns	Microns	Microns to millimetres	Nanometres to hundreds of microns
Morphologies	Many (<i>e.g.</i> , beads, core-shell, porous)	Some (<i>e.g.</i> , cylindrical, dumbbell)	Some (<i>e.g.</i> , core-shell, twisted)	Some (<i>e.g.</i> , hollow, triangle)	Various (<i>e.g.</i> , helical, core-shell, porous, knotted, triangle)

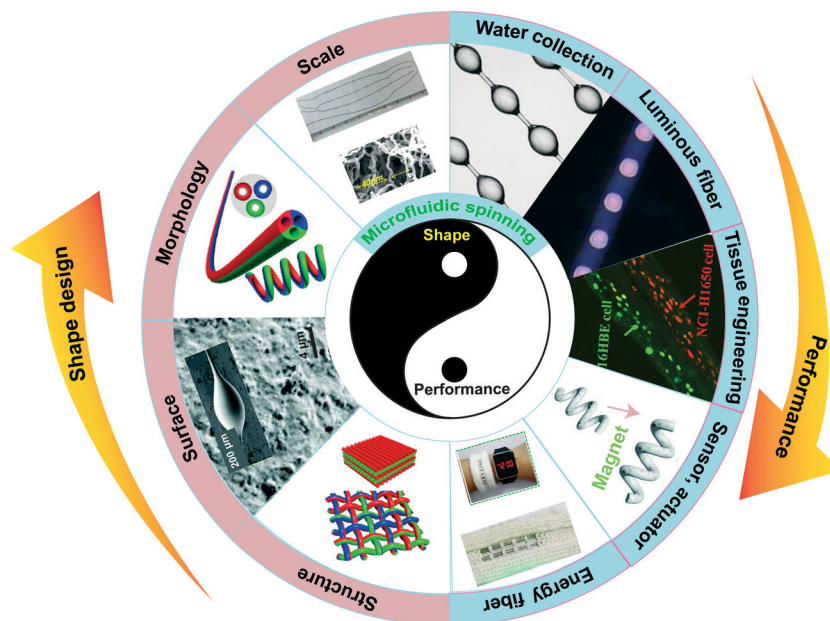


Fig. 1 Overview of the relationship between the fiber shape characteristics controlled by microfluidic spinning and the various types of fiber devices facilitated by the shape design. Images reproduced with permission: morphology^{4,5} Copyright 2016, American Chemical Society. Copyright 2017, Wiley-VCH. Scale/dimension,^{8,9} surface³ Copyright 2017, Wiley-VCH. Structure¹⁰ Copyright 2014, American Chemical Society.⁶ Copyright 2016, Wiley-VCH. Sensor, actuator.⁵ Copyright 2018, Wiley-VCH. Water collection.³ Copyright 2018, Wiley-VCH. Luminous fiber.¹¹ Copyright 2018, Royal Society of Chemistry. Energy fiber.⁴¹ Copyright 2017, Wiley-VCH. Tissue engineering.⁵¹ Copyright 2018, Wiley-VCH.

available and the chip does not require sophisticated equipment. Furthermore, glass capillaries are usually hydrophilic and their surfaces are easily modified for better fiber generation using various materials. Capillary-based devices provide versatile 3D flow channels, where the capillary module can be reconfigured to achieve the desired design.⁶² Several microfluidic systems have been developed, such as simple injection capillary microfluidics for the spinning of uniform microfibers (Fig. 2a), hierarchical injection capillary microfluidics for the spinning of core-shell or spindle-knot-structured microfibers (Fig. 2b), and multi-barrel injection capillary microfluidics for the spinning of microfibers with multiple components.⁶ In addition, microfluidic capillaries were used to control the template configuration and oil-core spillage, resulting in hourglass-shaped microfibers with tuneable morphologies and densities ranging from cavity microfibers to spindle microfibers.¹² Stainless-steel tubes have been used to prepare coaxial flow chips by carefully assembling the tubes with glass capillaries and precisely machining the spinneret (Fig. 2c).²¹ Although capillary-based microfluidic platforms do not require expensive equipment and are advantageous for generating coaxial round flows, the preparation of pulled-glass micropipettes is labour intensive and requires a high skill level.

The other main category of microfluidic spinning chips is based on plane patterning.^{63,78,84} Moulding techniques and/or photolithography are used to produce chips with various high-precision complex patterns. These chips use arrays of microchannels to fabricate parallel multiple Janus

fibers. A PDMS micro-device was prepared using standard soft lithography and replica moulding techniques (Fig. 2d), where the microchannel consisted of six rectangular inlet channels and a straight gelation microchannel to spin anisotropic calcium alginate (CaA) hydrogel fibers.⁵² As the gelling direction of this system is not uniform over the cross-sectional area, the rectangular microchannel configuration supplies Ca^{2+} ions only along the horizontal direction in the microchannel, while the alginate flow with an initial rectangular cross-section shapes the hydrogel fiber from both sides. Therefore, fibers with an anisotropic morphology and orientation were developed. In addition, a PDMS microfluidic chip was prepared using a rapid prototyping method with a single-layer membrane valve and digital controller (Fig. 2e).¹⁷ Two different droplet types were incorporated simultaneously into the fiber in a controlled way to produce biomimetic bamboo-like hybrid microfibers.

In nature, heterotypic materials with spatiotemporal changes in composition and morphology on the micro/nanoscale are common. The two aforementioned microfluidic spinning systems have been used in biomimetic chips to imitate silkworm and spider glands for fiber spinning.^{86–90} Inspired by the hierarchical structure of silk fibers and the silkworm spinning process (Fig. 2f), a multi-channel microfluidic platform was developed to spin multicomponent carbon nanotube (CNT) microfiber supercapacitors (Fig. 2g).¹⁸ Inspired by the spinning of spider silks (Fig. 2h), biomimetic microfibers with desirable morphology and structure were produced using a

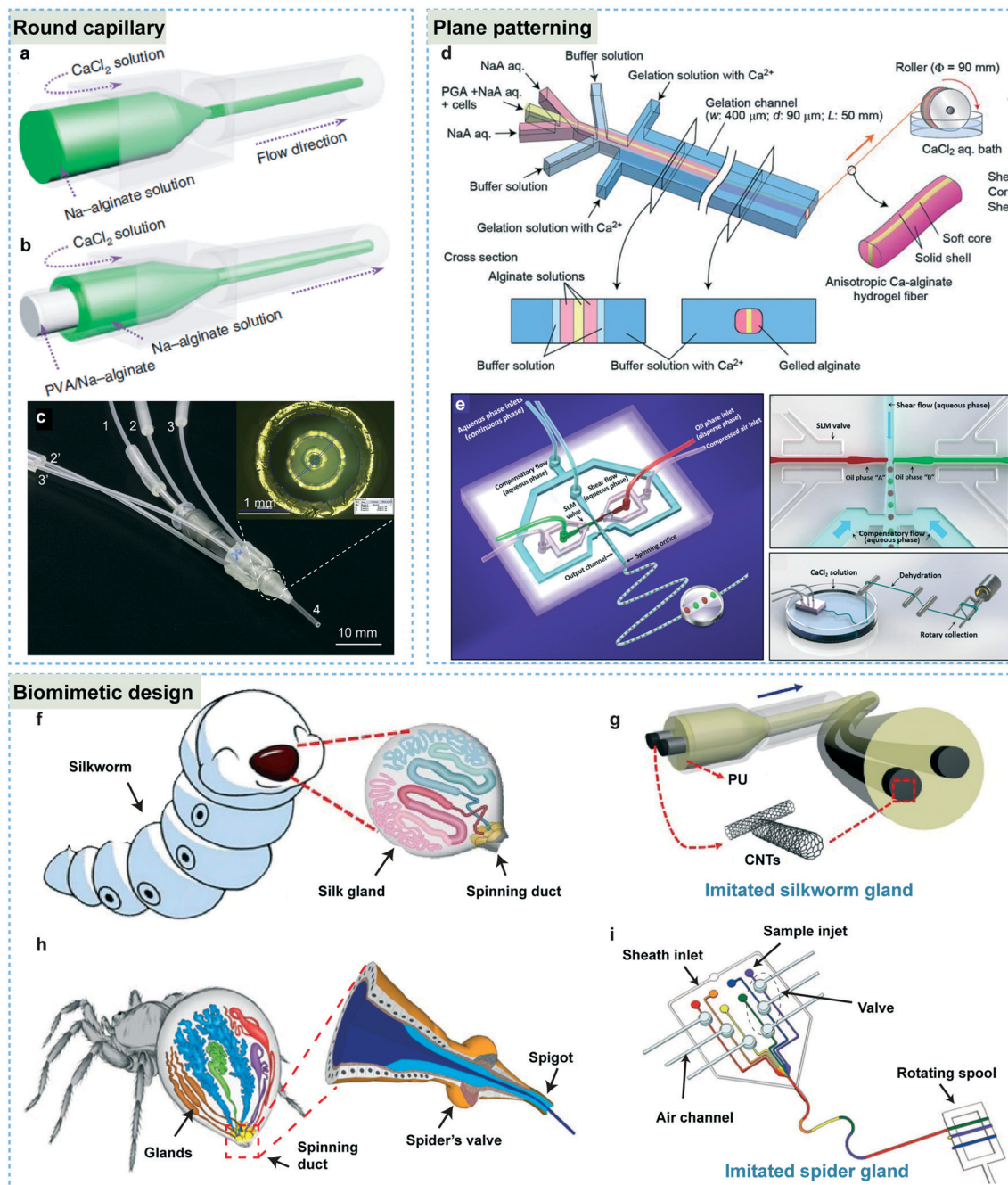


Fig. 2 Microfluidic chip systems for fiber formation. Round capillary-based chip for microfluidic spinning: (a) simple and (b) core-shell-structured microfluidic chip for sodium alginate fiber spinning. Reproduced with permission.⁶ Copyright 2018, Springer Nature. (c) Triple-orifice spinneret based on a round stainless-steel tube. Reproduced with permission.²¹ Copyright 2010, Elsevier Publishing Group. Plane chip for microfluidic spinning based on a surface patterning design: (d) microfluidic system based on PDMS microdevices fabricated by taking advantage of standard soft lithography and replica mold technology to synthesize anisotropic CaA hydrogel fibers. Reproduced with permission.⁴⁵ Copyright 2012, Royal Society of Chemistry. (e) A microfluidic chip fabricated in PDMS by the rapid prototyping method for CaA microfiber spinning. Reproduced with permission.¹⁷ Copyright 2014, Wiley-VCH. Biomimetic microfluidic chip design: (f) diagram of natural silkworm spinning and (g) the corresponding biomimetic microfluidic spinning device for multicomponent CNT microfibers. Reproduced with permission.¹⁸ Copyright 2020, Elsevier Publishing Group. (h) Diagram of a spider spigot and (i) the corresponding biomimetic microfluidic spinning chip for hydrogel microfibers. Reproduced with permission.⁷⁰ Copyright 2011, Springer Nature.

microfluidic system consisting of a digital flow controller.⁷⁰ In addition, hydrogel microfibers with varying chemical composition and topography along the fiber were produced, including gas micro-bubbles and nanoporous spindle knots

that have directional water-collection functionality. Hence, these microfluidic chips in various forms enable the biomimetic fiber spinning, giving them different shape characteristics and properties.

2.2 Microfluidic principles for fiber formation

The most popular method for fiber device fabrication by microfluidic technology is based on laminar flows in the microchannels.⁶² With a low Reynolds number, two or more flows form a stable laminar flow regime inside the microfluidic chips, with only ion exchange, diffusion and/or solvent vaporisation. If the spinnable polymer can be solidified during the flow process or directly at the outlet of the microfluidic chip, continuous fibers can be obtained from the microfluidic chips. Therefore, microfluidic chips generally require a basic core-shell structure, with the core polymer being solidified by the reaction with a shell fluid during laminar flow or under ultraviolet (UV) irradiation. Photopolymerization is usually achieved by combining the UV-polymerizable backbone material with a photoinitiator before injection.⁹¹ After the prepolymer is introduced into a round microfluidic channel, the scaling effects lead to the generation of a coaxial flow with a central prepolymer flow and a shell flow. The shell flow functions as a lubricant to promote fiber extrusion. Using this method, 4-hydroxybutyl acrylate (4-HBA) fibers were fabricated, where the photopolymerizable 4-HBA mixed with a dye was used in the core flow and a non-polymerizable material (PVA and DI water) was used in the shell flow. The moving liquid was exposed to UV radiation (365 nm) as it flowed through the channel.⁹² In this system, the polymerization process is simple and stable, but limited to materials for engineering applications, which are not biodegradable or sensitive to UV radiation (unlike bioactive species). For the regenerated spun fiber with chemical cross-linking, the spinnable polymer flows in the core while the second phase for solidification flows in the outside channel with a controlled speed. By this method, cylindrical alginate fibers were produced using an alginate solution as the core flow and an aqueous CaCl₂ solution as the shell flow.⁹³ At the interface between the two flows, sodium alginate (NaA) is cross-linked because of the diffusion of Ca²⁺ ions into the alginate solution. Similarly, Zhang *et al.* used SrCl₂ as the shell flow to produce Sr-alginate (SrA) hydrogel fibers with the microfluidic spinning technique.⁹⁴ They investigated the chain linkage model and discussed metal-alginate dimer conformation. SrA fibers had better mechanical performance than CaA ones due to the strong binding of Sr²⁺ with the alginate molecular chain.

Another microfluidic chip for fiber spinning requires only one fluid channel, where fiber solidification occurs in the processing environment or *via* a post-treatment step.⁹⁵ This method requires a spinning aid that is easy to spin and facilitates solidification. Xu *et al.* used microfluidic spinning to produce fluorescent-dye-doped PVP microfibers, which were then woven to produce multi-coloured patterns of parallel arrays and grids.⁹⁶ Li *et al.* used a homogeneous mixture of viscous PVP and monodisperse SiO₂ particles to fabricate microscale fibers.⁴⁷ By controlling the speed of the microfluidic spinning motor, fibers with various diameters were produced efficiently. The monodisperse SiO₂ particles

were assembled into photonic-crystal structures with bright structural colours by removing the PVP through calcination. The colour was easily controlled by adjusting the size of the SiO₂ colloid particles. This spinning method is similar to gel-dry spinning.

In addition, microfluidic patterning based on soft lithography is commonly used for fabricating nanowires with high uniformity and controllable sizes. For example, ZnO nanowires can be fabricated using a PDMS chip with 3D microchannels by an eco-friendly, inexpensive, and facile hydrothermal reaction. The geometric and mechanical properties of these ZnO nanowires were further used for mechanical cell lysis.⁹⁷ Chen *et al.* developed a facile method to fabricate nanowires by controlling the flow direction of semiconductor solutions inside the PDMS nanochannels and successfully fabricated well-aligned semiconductor nanowires with different materials, including p-type and n-type polymers, which can be utilized for fabricating field-effect transistors (FETs).

3. Shape characteristics of microfluidic fibers

3.1 Scale

Scale refers to the size range of the fiber geometry and is an important factor contributing to the structure and properties of fiber materials and devices.²³ The fiber diameter dramatically affects its specific surface area (S_s):

$$S_s = \frac{S_f}{V_f} \Rightarrow \frac{P \cdot l + 2A_f}{V_f} = \frac{4}{d} + \frac{2}{l} \approx \frac{4}{d} \quad (1)$$

where S_f and V_f refer to the fiber surface area and volume, respectively. In the case of a circular fiber cross-section, P is the perimeter, l is the fiber length, A_f is the cross-section area, and d is the fiber diameter. In the case of a circular fiber cross-section with a large aspect ratio ($l \gg d$), this relationship can be simplified, as shown. As shown in Fig. 3a, S_s increases dramatically when d decreases from the microscale (1–100 μm) to submicron scale (0.1–1 μm), while it increases by orders of magnitude at the nanoscale (1–100 nm). Such changes in d (and hence, S_s) affect the fiber properties in many ways. When the fiber becomes thinner and more of the total volume of the material is at the surface, the adsorption and interaction with nearby materials are enhanced. Second, it becomes easier to heat and cool the fibers. Third, the enhanced curvature of the reflective surfaces of the fiber can increase light scattering and internal multiple refractions and reflections, which may change the fiber colour. Fourth, thinner fibers are easily solidified during spinning.

3.1.1 Nanofibers. The formation of ultrathin fibers requires high processing precision, especially for submicron and nanoscale fibers. By carefully designing the microfluidic spinning chips and controlling the spinning parameters, nanofiber spinning has been achieved.²⁸ Alginate nanofibers with a highly ordered structure were produced using a

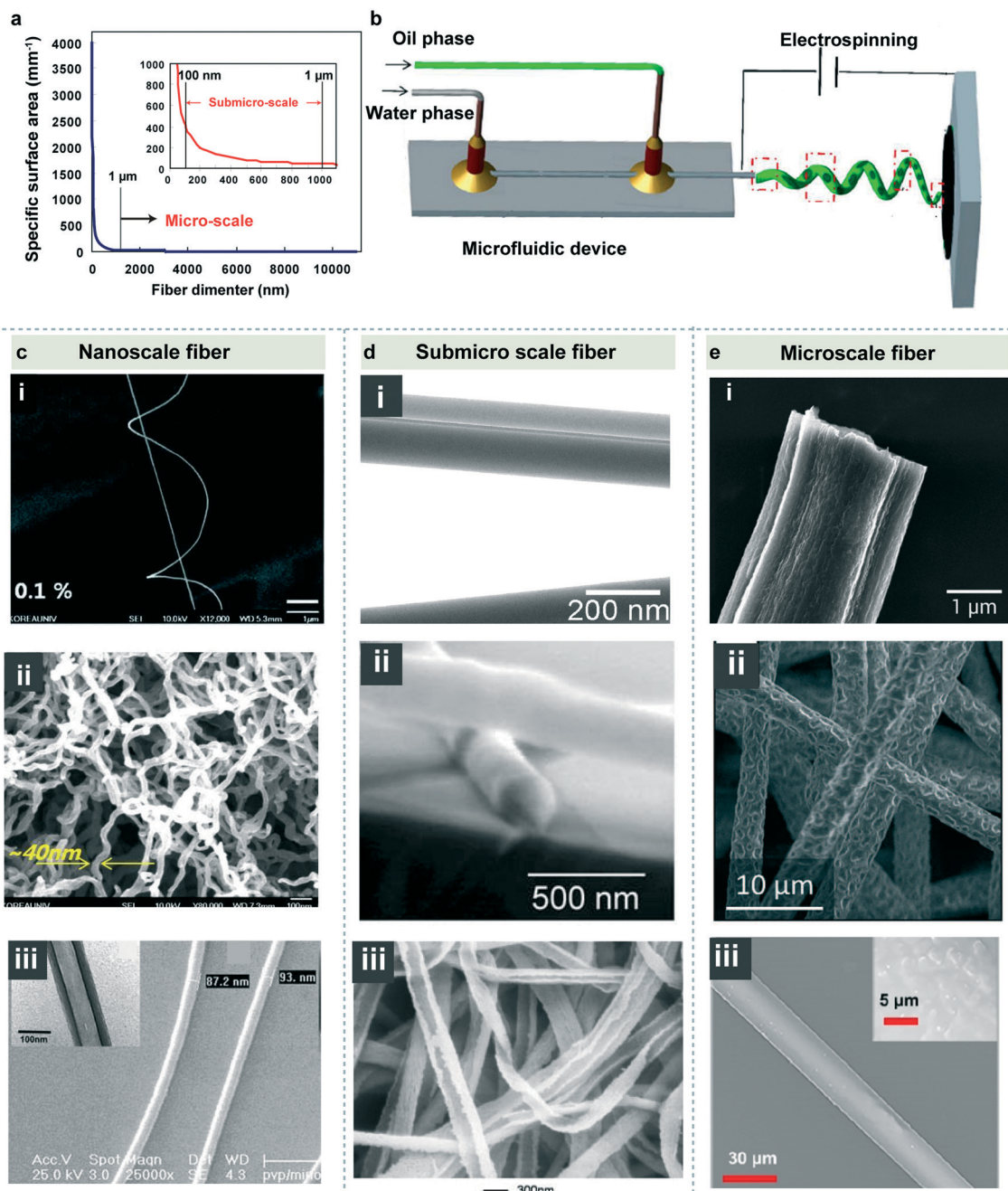


Fig. 3 Dimensional properties of fibers fabricated by microfluidic spinning. (a) Specific surface area as a function of the fiber diameter from the nanoscale (1–100 nm), submicron scale (0.1–1 μm), and microscale (>1 μm). (b) Schematic of a microfluidic electrospinning device for fabricating nanofibers. Reproduced with permission.⁷ Copyright 2018, American Chemical Society. (c) Microfluidic spun nanoscale fibers: (i) SEM images of alginate nanofibers spun by the microfluidic method with isopropyl alcohol (IPA) shell flow to mimic the spinning process of silkworms, (ii) self-aggregated solid mass of nanofibers in IPA. Reproduced with permission.⁹ Copyright 2013, Wiley-VCH. (iii) SEM and TEM image (inset) of the hollow nanofibers of PVP + TiO₂ obtained by electrospinning using a microfluidic manifold. Reproduced with permission.²⁸ Copyright 2008, Springer Nature. (d) Microfluidic spun submicron fibers: (i) TEM image of PVP + PPY/PVP bicomponent nanofibers. Reproduced with permission.³⁷ Copyright 2009, American Institute of Physics. (ii) SEM image of hollow fibers of PVP and TiO₂. Reproduced with permission.⁴⁸ Copyright 2008, Springer Nature. (iii) SEM image of a co-spun PAN/PU fiber after dissolution of the PU core. Reproduced with permission.⁵³ Copyright 2005, Wiley-VCH. (e) SEM images of microfluidic spun microscale fibers: (i) surface topology of an individual PAN fiber with a diameter of 2.7 μm. Reproduced with permission.⁵⁸ Copyright 2018, Royal Society of Chemistry. (ii) A fiber containing perfluorinated copolymers and polycaprolactone. Reproduced with permission.⁶⁷ Copyright 2018, Royal Society of Chemistry. (iii) SEM image of a BSA fiber. Reproduced with permission.⁶⁹ Copyright 2020, Wiley-VCH.

microfluidic spinning method that mimics that of a silkworm.⁹ Highly aligned fibers with lots of ordered

nanostrands were fabricated at the dehydrating interface between the isopropyl alcohol (IPA) shell fluid and the

aqueous polar core by dipole–dipole attractions. The shearing effect in the microfluidic channel facilitated the alignment of polymer chains to form a dense structure, which enabled the fiber diameter to be decreased to nanometres (Fig. 3c(i) and (ii)).

Another common method for fabricating microfluidic fibers is combining microfluidic chips with electrospinning. As shown in Fig. 3b, the microfluidic flow was controlled by the chip while an electrostatic generator in the spinneret was used to draw the fibers after the preforms coming out from the outlet.⁷ By this method, hollow and core/shell nanofibers were fabricated with a PDMS microchip device and electrospinning.²⁸ The as-prepared hollow poly(vinylpyrrolidone) (PVP) and TiO₂ composite nanofibers had a diameter of 100 nm. In addition, nanofibers spun from PVP with 10% FeCl₃ had a smaller average diameter (~100 nm) than those without FeCl₃ (~250 nm), as the higher solution conductivity increased the electrical force acting on the jet, causing the fiber to elongate during electrospinning.⁹⁸ Aside from electrostatic drawing, other drafting effects can be also applied to combine with microfluidic chips for fiber spinning. For example, by combining traditional microfluidic spinning with air blowing,^{99,100} nanofibers can be fabricated. This method is called microfluidic blowing-spinning.^{38,101}

3.1.2 Submicron fibers. Submicron fibers (with a diameter of 0.1–1 μm) can also be achieved using microfluidic spinning chips. As the equipment requirements are less stringent than those for producing nanoscale fibers, there are more research results within this scale range. Using an elastomeric microfluidic device together with electrospinning, biphasic Janus nanofibers of polypyrrole (PPy)/PVP with an average diameter of 250 nm were produced (Fig. 3d(i)).³⁷ Using the same method, hollow submicron PVP/TiO₂ fibers were fabricated (Fig. 3d(ii)).⁴⁸ Additionally, a microfluidic electrospinning apparatus was developed for co-electrospinning two polymer solutions side-by-side.⁵³ The as-spun polyacrylonitrile/polyurethane (PAN/PU) fibers had curled and helically crimped fiber morphologies. The average fiber diameter was 240 nm, where some fibers were so tightly curled that the diameter of the helix was as small as 500 nm. After dissolving PU in tetrahydrofuran (THF), the remaining PAN fiber showed a U-shaped cross-section (Fig. 3d(iii)). Kameoka *et al.*¹⁰² fabricated oriented polymeric nanofibers by combining electrospinning deposition with an integrated microfluidic chip. A microfabricated triangular tip was used at the microfluidic channel outlet to generate a source that could be close to the counter electrode. By taking advantage of the orientation ability of the nanofibers, 140 nm-diameter suspended ordered fibers were formed on the substrate. This method has potential applications in the rapid formation of molecular electronic architecture and transparent conductive electrodes.^{32,103,104}

3.1.3 Microfibers. Microfluidic spinning is commonly used for fabricating microscale fibers (1–100 μm) and has been used to produce microfibers with different morphologies and

components. Lölsberg *et al.* developed a wet-spinning process by miniaturization of a spider-inspired spinneret nozzle for producing wet-spun monofilaments with the dimensions of natural spider silk.⁵⁸ The as-prepared PAN fiber had a diameter of 2.7 μm (Fig. 3e(i)). Hofmann *et al.*⁶⁷ designed a microfluidic nozzle for fabricating uniform fibers with practically unlimited length continuously while accurately controlling the fiber diameter (Fig. 3e(ii)). The nozzle was used to produce ultrafine fibers of perfluorinated copolymers and polycaprolactone, which were collected on a rotating cylinder. Further, robust protein fibers were fabricated from bovine serum albumin (BSA) using a microfluidic technique (Fig. 3e(iii)).⁶⁹ These fibers had a high toughness and breaking strength that are comparable to or even higher than those of many regenerated silk fibers.

The refinement of the fiber diameter is a challenging but necessary topic in fiber spinning. The combination of microfluidic spinning with other external physical fields provides new opportunities for nanoscale fiber spinning. Although some nanoscale fibers have been successfully regenerated by carefully controlled microfluidic spinning, most studies have presented submicron or microscale fibers. Future research should focus on manipulating the fiber scale to improve the fiber performance.

3.2 Morphology

In the case of microfluidic spun fibers, the morphology refers to the geometry along the fiber surface. According to the macroscopic morphology, microfluidic fibers are classified into cylindrical, profiled, hollow, heterogeneous, helical, and knotted fibers, among others.

3.2.1 Cylindrical fibers. Cylindrical fibers (Fig. 4a) are most commonly prepared using microfluidic devices as they can be produced using simple spinning chips and easily controlled processing conditions.^{92,105,106} During microfluidic spinning, the spinnable component should be quickly solidified at the spinneret. To produce cylindrical fibers, a core–shell structured microfluidic spinning apparatus is commonly used in combination with solidification methods such as photopolymerization or chemical reactions.¹⁰⁷ For photopolymerization achieved by combining the UV-polymerizable backbone material with a photoinitiator before injection, cylindrical fibers of poly(ethylene glycol) diacrylate (PEG-DA), 4-HBA,⁹² and PU¹⁰⁸ with the help of shell shaping have been reported. For the regenerated spun fiber with chemical cross-linking, the spinnable polymer flows in the core while the second phase for solidification flows in the outside channel with a controlled speed. Using this method, cylindrical alginate fibers were produced using an alginate solution as the core flow and an aqueous CaCl₂ solution as the shell flow.⁹³

3.2.2 Profiled fibers. Profiled fibers have irregular cross-sections, which can be achieved using microfluidic spinning channels with specific cross-sectional shapes, flow control, and spinning with a liquid template. Microfluidic spinning

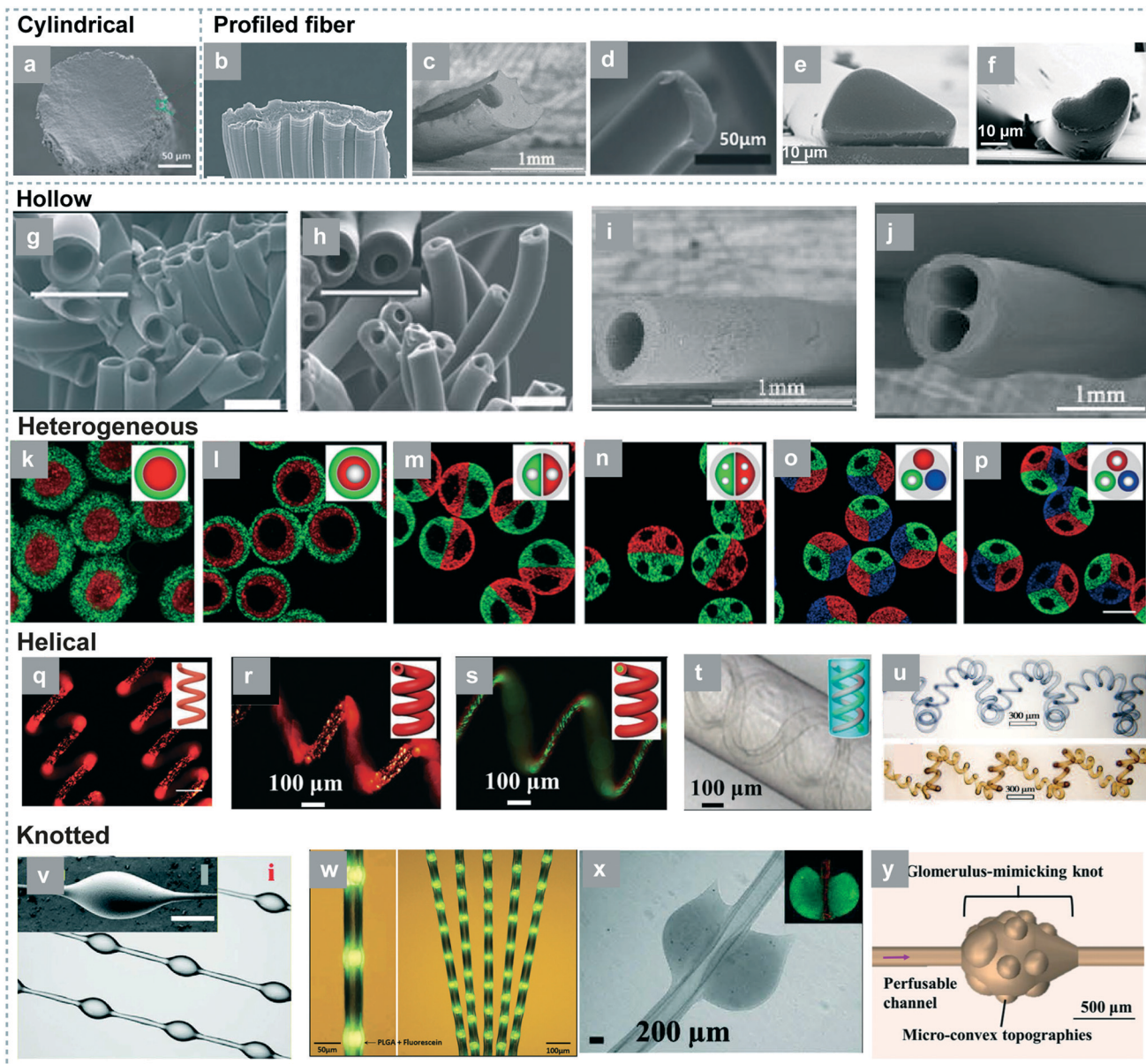


Fig. 4 Morphologies of microfluidic fibers. (a) Cylindrical fiber. Reproduced with permission.¹⁴ Copyright 2018, Royal Society of Chemistry. Profiled fibers with different cross-sectional shape characteristics: (b) grooved rectangle, reproduced with permission.²⁰ Copyright 2012, Wiley-VCH. (c) Maple leaf, reproduced with permission.⁵² Copyright 2017, Elsevier Publishing Group. (d) Crescent, reproduced with permission.⁵⁷ Copyright 2011, Royal Society of Chemistry. (e) Triangle, reproduced with permission.⁶⁸ Copyright 2014, Wiley-VCH. (f) Kidney bean. Reproduced with permission.⁶⁸ Copyright 2014, MyJove Corporation. (g and h) Hollow fibers with different core diameters. Reproduced with permission.⁵⁷ Copyright 2011, Royal Society of Chemistry. (i and j) Hollow fibers with one or two pores. Reproduced with permission.⁵² Copyright 2017, Elsevier Publishing Group. Heterogeneous fibers: (k) core-shell structure, reproduced with permission.⁵ Copyright 2018, Springer Nature. (l) Hollow fiber with two shell layers, reproduced with permission.⁸⁰ Copyright 2014, Wiley-VCH. (m and n) Bilateral hollow fibers with different cores, reproduced with permission.^{4,6} Copyright 2018, Springer Nature. Copyright 2016, American Chemistry Society. (o and p) Three-component hollow microfibers with different cores. Reproduced with permission.⁴ Copyright 2016, American Chemistry Society. Helical fibers: (q) simple helical fiber, reproduced with permission.¹³ Copyright 2017, Wiley-VCH. (r) Hollow helical fiber, reproduced with permission.¹³ Copyright 2017, Wiley-VCH. (s) Core-shell helical fiber, reproduced with permission.¹³ Copyright 2017, Wiley-VCH. (t) Double-helical microfibers, reproduced with permission.¹³ Copyright 2017, Wiley-VCH. (u) Superhelical fiber. Reproduced with permission.⁸⁵ Copyright 2019, Wiley-VCH. Knotted fibers: (v) simple knotted fiber, reproduced with permission.³ Copyright 2017, Wiley-VCH. (w) Bamboo-like fiber, reproduced with permission.¹⁷ Copyright 2014, Wiley-VCH. (x) Petaloid-like fiber, reproduced with permission.⁷⁷ Copyright 2018, Wiley-VCH. (y) Glomerulus-like knot fiber. Reproduced with permission.²⁴ Copyright 2020, American Chemistry Society.

chips with channels of irregular cross-sectional shapes are commonly used for profiled fiber fabrication.⁷⁷ Kang *et al.* fabricated the first microscale grooved fiber in the form of

alginate microribbons with controllable grooved microstructures with a microfluidic system (Fig. 4b).^{20,109} The microfluidic spinning chip was composed of two channels,

where the core channel had a grooved structure. By placing various PTFE rods or tubes in one capillary, the microfluidic chip can be used to spin shaped fibers. Profiled polyacrylamide (PAM) fibers with C-shaped, double-anchor, and maple-leaf cross-sections have been produced (Fig. 4c).⁸⁶

Profiled fibers can be fabricated by combining target materials with a soluble spinning material that is removed after spinning to leave the insoluble profiled fiber. By controlling the spreading coefficients and evolution time in the downstream part of the microfluidic system, profiled microfibers with different components can be formed with various shape characteristics after dissolution of one component. Fibers with complex profiles were produced using different liquid template streams as well as a polymerizing stream together with the outer oil phase co-flowing through the cross-junction.⁵⁷ The polymerized regions formed a permanent structure while the liquid template stream was dissolved by the organic solvent or water. Using this method, profiled fibers with crescent cross-sections were developed (Fig. 4d).

Another method to fabricate profiled fibers with irregular cross-sections is based on hydrodynamic focusing using a shell stream to shape the prepolymer stream. For multi-channel microfluidic devices with coaxial flow, grooves inside the microfluidic channel were designed to manipulate the shell fluid flow and shape the core one. Controlling the relative flow rates of the shell and core fluids determines the cross-sectional area of the core fluid. Polymerization of the core fluid enabled the generation of a profiled fiber downstream from the shaping region. Using this method, hybrid fibers with predesigned sizes and shape characteristics, including triangular and kidney-bean cross-sections, were fabricated (Fig. 4e and f).⁶⁸

3.2.3 Hollow fibers. Hollow fibers are a special profiled fiber with cylindrical holes along the axial direction of the fiber, which are fabricated using a similar spinning method to those used for other profiled fibers. Highly uniform and hollow structured PEG fibers (Fig. 4g) with a clear interface between the core and the shell region were produced using 100% PEG-DA solution without a photoinitiator as the core flow and 50% PEG-DA with 8% photoinitiator as the shell flow.⁵⁷ The liquid template in the core region that was not polymerized was dissolved after spinning. The dimensions of the core and shell parts were controlled *via* adjusting the flow rates of the liquid template as well as the polymerizing fluid. Therefore, fibers with different core diameters can be fabricated (Fig. 4h). Using microfluidic spinning chips with empty channels inside the circular fiber spinning channel, hollow fibers with one or two cores were obtained. Liu *et al.* designed a microchannel by inserting one or two small polytetrafluoroethylene (PTFE) capillaries in the centre of a large PTFE capillary, enabling the preparation of hollow PAM fibers with one or two hollow cores.⁵² The PEG/acrylamide (AM) solution was injected into the large capillary. After polymerization, PAM fibers with round central cores were produced (Fig. 4(i and j)).

3.2.4 Heterogeneous fibers. Heterogeneous fibers contain different features in a single fiber. Complex microfibers with multiple channels and components have been produced using multi-barrel capillaries^{4,6,80} or membrane microchips^{51,110} to construct complex laminar-flow microfluidic devices. Various multicomponent microfibers were produced from multi-flows of NaA and CaCl₂ solutions by immediate microfiber gelation at the orifice of the capillary, which was coaxially aligned with a round capillary for collection inside a square capillary.⁸⁰ By adjusting the injection capillary design, heterogeneous microfibers with an anisotropic multicomponent body, core, and shell composition were formed. Microfibers with core-shell structures (Fig. 4k) were spun with round capillary-based chips.⁶ Similarly, two-shell (Fig. 4l) and three-shell hollow microfibers were fabricated.⁸⁰ In addition, bilayer fibers with multiple hollow cores in each component were continuously spun (Fig. 4m and n).^{15,39} Three-component hollow microfibers with different numbers of cores were also fabricated using the capillary assembly.³⁹ In addition, membrane-sandwiched three-layer microchips with different patterns were produced using standard soft lithography etching methods for multicomponent heterogeneous microfiber production. In addition, one-, two-, and three-component microfibers were fabricated using a two-layer microchip, while four-component microfibers with various structures were fabricated using a membrane-sandwiched three-layer microchip.⁵¹

3.2.5 Helical fibers. Helical fibers were obtained by controlling the flow rates of the microfluidic device,^{39,78,79} where the liquid jet tends to form a helical structure with a random rotating direction inside the collection channel when a critical flow-rate ratio is reached.¹³ When the ratio of the inner flow rate to the outer flow rate increases, the inner liquid jet will deform and buckle, resulting in a helical structure. Yu *et al.* fabricated simple helical fibers (Fig. 4q) by controlling the flow rate of NaA and CaCl₂ solutions.¹³ In addition, modifying the injection capillary design of the microfluidic chip, various helical fibers, such as hollow (Fig. 4r), core-shell (Fig. 4s), and double (Fig. 4t) helical microfibers, were fabricated. The spinning chip designs are similar to those used for producing heterogeneous fibers, although with flow rate control of the core and shell liquids.

3.2.6 Knotted fibers. Microfluidic spinning also provides a method for the fabrication of knotted fibers by controlling the composition and flow rate of the different fluids. Shang *et al.* used a coaxial microfluidic chip that contained an inner, middle, and outer capillary to fabricate microfibers with spindle knots.³ The core NaA liquid flow was injected into the middle pregel phase with Ca²⁺, which formed a flow shell and functioned as a coating layer on the generated microfiber surface. The shell layer was then emulsified with an immiscible outer fluid and formed spindle-shaped knots on the microfiber. The emulsification process is precisely controllable by adjusting the flow rates; therefore, the size and spacing of the spindle knots is highly tuneable. The knot

morphology has an important effect on the water collection ability of the fiber.

A plane-based chip that combined three flow channels was used to fabricate bamboo-like fibers (Fig. 4w)¹⁷ with joints of poly (lactic-co-glycolic acid) (PLGA) spheres with fluorescein (GFP) and CaA microfibers as the continuous part. An aqueous solution was used to shear the oil phase to form droplets at the “T” junction, while a side-channel downstream of the cross-junction geometry was used as the compensatory flow to adjust the aqueous-phase flow rate for the subsequent fiber spinning. The size and spacing of the spindle knots on the microfibers were highly controllable. In addition, hemisphere-knotted or petal-like knotted fibers were also developed by microfluidic spinning.³² Knotted fibers were fabricated using a vertically oriented coaxial microfluidic device with CaCl₂ as the core fluid and a mixture of CaCO₃ powder in an alginate solution as the sheath fluid. Owing to the diffusion of Ca²⁺ ions, a thin gelatinized CaA layer was immediately formed around the core flow, creating a hollow channel. The non-crosslinked NaA generated droplets that dripped from the capillary end to form periodic spindle knots. In addition, hemisphere-knotted microfibers were produced by simply altering the direction of fiber collection from vertical to horizontal. By combining two spinning devices obliquely with their tips in contact, petal-like knotted fibers were fabricated (Fig. 4x).³²

Xie *et al.* fabricated biomimetic 3D glomeruli based on a hollow fiber with glomerulus-like knots of microconvex topography for podocyte cultivation (Fig. 4y).⁷⁷ The non-crosslinked alginate solution accumulated and formed a droplet at the tip of the capillary and dripped regularly to form spindle knots on the hollow microfiber. The microconvex topography on the fiber surface was then fabricated by a chemically induced inflation method, similar to that used to form soap bubbles by expanding air inside a soap solution.²⁴ This process for forming knotted fibers by microfluidic spinning provides opportunities for the development of biomimetic tissues.

Although microfluidic spinning technology has many advantages for controlling the fiber shape characteristics and has been widely used to fabricate fibers with various morphologies, the range of spinnable materials, and subsequent applications, are limited. Further studies of fibers produced from proteins, cellulose, and other polymers with different morphologies should be performed in the future.

3.3 Surface

The fiber surface texture and structure have a decisive effect on the surface properties, such as friction and wetting. Friction occurs on the surface when the fibers move against each other or over the surface of a substrate. The wetting properties determine the affinity of the fiber with a certain liquid. If the liquid is solidified on the surface of the fiber or directly coated on the fiber, the adhesion mechanism will be more important.

Many researchers noticed the significance of the fiber surface on its performance and intentionally tailored the surface structure using microfluidic chips. For example, the surface roughness has a direct effect on the fiber performance.¹¹¹ Kang *et al.* investigated cell movement on smooth and rough surfaces (Fig. 5a), where the migration of neuronal cells was retarded on grooved fibers compared to smooth ones; most neuronal cells aggregated to form networks across the fibers and many adhered to the groove ridges due to the higher frictional resistance of rough surfaces (Fig. 5b–d).²⁰ In addition, smooth and grooved fibers with micropatterned surfaces were produced using a microfluidic chip with flat and grooved patterns inside the channel wall (Fig. 5e and f).²² Such fiber surface micropatterns were shown to enhance the generation of bioengineered muscle tissue, such as in the case of microfibers with spindle knots formed from droplets of a colloidal suspension of polystyrene (PS) nanoparticles (Fig. 5g), which acted as solid photonic crystals with stable structural colours.³ The rough surface provided by the knots is also favourable for cell cultivation, such as glomerulus-like knots with microconvex surface topography for podocyte cultivation (Fig. 5k).²⁴

Controlling the surface structure is also useful for tailoring the wetting properties of the fiber. Bio-inspired knotted fibers were fabricated with a smooth surface on the continuous joint sections and a rough surface with many pores on the knotted segments (Fig. 5i and j).^{3,46} The different surface structures of the fiber and knots provide a gradient in the wettability force and curvature, which results in a Laplace pressure difference¹¹² that enables fog capture or water collection. Therefore, modification of the fiber surface characteristics plays an important role in providing functionality for water collection, luminosity, and tissue engineering applications.

3.4 Structure

Here, structure refers to the orientation, stacking density, and interaction between the basic units (*e.g.*, molecules, nanoparticles, fibrils, fibers, or yarns) in textile materials. The orientation occurs at different scales, such as between the basic nanofibers during spinning and fiber alignment after spinning. The stacking density is the number or mass of basic units per unit volume, such as the amount of nanoparticles distributed on a unit surface. The interactions between the basic units, such as the adhesion and friction between fibrils and fibers, contribute to the overall fiber structure. The importance of these factors in microfluidic spinning is discussed in this section.

3.4.1 Orientation. The orientation of the basic units is an important factor determining the structure and properties of the final fiber or fiber assembly. The ordering at different scales, such as the nanofibrils, particles within/on the fiber, and the final fibers themselves, is important to the performance. First, microfluidic spinning enables precise

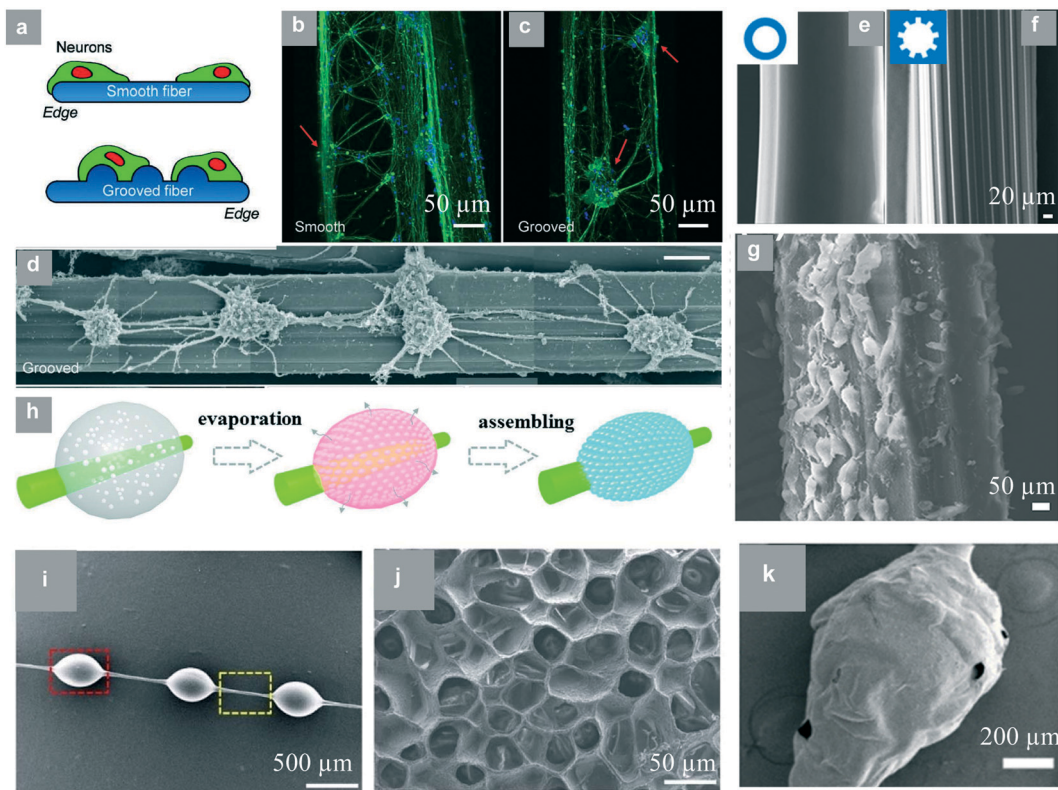


Fig. 5 Fiber surface manipulated by microfluidic spinning. (a) Schematic illustration and (b–d) SEM images of neuron cells on the surfaces of (b) smooth and (c and d) grooved fibers. Reproduced with permission.²⁰ Copyright 2012, Wiley-VCH. (e and f) Schematic illustration and SEM images of spun fibers with smooth and grooved surfaces. Reproduced with permission.²² Copyright 2018, Springer Nature. (g) SEM image of a grooved fiber after 3D of cell culture. Reproduced with permission.²² Copyright 2018, Springer Nature. (h) Schematic illustration of microfibers with knots of colloidal PS suspension droplets forming as the water evaporates. Reproduced with permission.³ Copyright 2017, Wiley-VCH. (i) The surface morphology of a biomimetic fiber and higher-magnification images of (j) the knotted section. Reproduced with permission.⁴⁶ Copyright 2017, Royal Society of Chemistry. (k) Microconvex topography of a glomerulus-like knot on a fiber surface. Reproduced with permission.²⁴ Copyright 2020, American Chemistry Society.

multiscale control during the assembly of nanoscale protein nanofibrils to spin micro- and macroscale fibers.^{1,2,9,113–116} The alignment of nanofibrils by shearing and elongation flows in the fluid channel is beneficial for producing fibers with good mechanical performance.¹¹⁵ To achieve good alignment of the nanofibrils in cellulose/regenerated silk fibroin (RSF) complex solutions, a microfluidic chip with gradually decreasing channel width was used,² where the shear flow can orient both the RSF chains and cellulose nanofibers (CNF) (Fig. 6a). With the further decrease of the channel diameter, the enhanced elongation flow greatly improved the orientation of CNF aggregates and caused conformation changes in the RSF chains due to the strong intermolecular interactions between the RSF and CNF. Kamada *et al.* applied a biomimetic microfluidic spinning method to precisely control nanofibril alignment (Fig. 6b).¹ By adjusting the shell flow rate, fibers with highly ordered nanofibrils (Fig. 6c and d) were achieved with an orientation index comparable to that of natural silk. The results showed that the elastic modulus of the regenerated fiber increased with increasing orientation degree of the nanoscale building blocks. In addition to the nano-fibril orientation, the obvious

shearing effect in the spinning channel will induce crystallization. In regenerated silk fiber spinning, the rapid extensional flow will initiate the fibroin structure into insoluble crystalline, which is another main important reason for its excellent macro performance.^{87,117} Hence, the fiber properties have a strong relationship with the nanofibril orientation.

In microfluidic spinning, different components in the heterogeneous fibers can be programmed to control the order of their deposition by adjusting drop valves in the chip.¹¹⁸ This process has been used to align colloidal crystals in fibers, and sequentially arrange particles with different colours in the knotted fiber. As shown in Fig. 6e, box-jellyfish-like hydrogel microfibers were produced, where the size, spacing, number, and sequence of different colloidal crystals were simultaneously controlled.¹¹ Yu *et al.* encoded the fiber with two liquids with different colours (Fig. 6f) by controlling single-layer membrane valves.¹⁷ Zhang *et al.* fabricated editable beaded polylactic acid (PLA) fibers with monodisperse multicore microspheres (Fig. 6g), which showed suitable mechanical properties and knittability for fabricating editable smart colour-changing

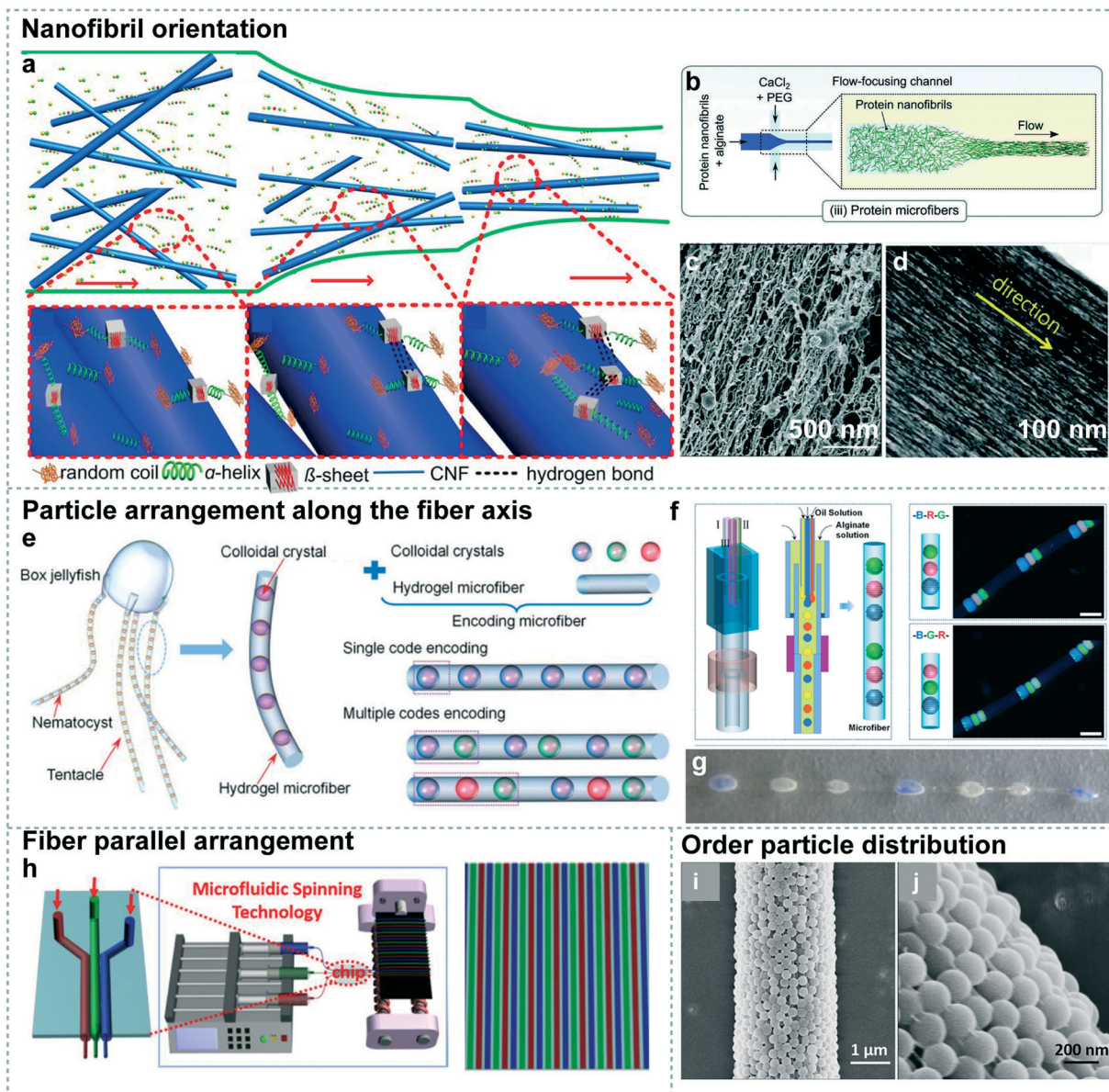


Fig. 6 Multiscale orientation by microfluidic spinning. (a) Schematic of the gradual orientation of fibrils in the RSF/CNF suspension along the microfluidic channel. Reproduced with permission.² Copyright 2019, American Chemistry Society. (b) Microfiber assembling through shear-induced alignment. Reproduced with permission.¹ Copyright 2020, Wiley-VCH. (c) SEM image of a hydrogel network being oriented along the fiber axis with high shell flow rates. Reproduced with permission.¹ Copyright 2020, Wiley-VCH. (d) TEM image of nanostrands oriented along the fiber axis direction. Reproduced with permission.¹ Copyright 2020, WILEY-VCH. (e) Schematic illustration of particle patterns along the fiber axis for microfiber colour encoding. Reproduced with permission.¹¹ Copyright 2019, Royal Society of Chemistry. (f) Images showing dehydrated CaA fibers encoded by two droplets with different colours. Inset: Encoding of the smallest repeating unit of droplets. Reproduced with permission.¹⁷ Copyright 2014, Wiley-VCH. (g) Photographs of beaded PLA fibers with blue-red order. Reproduced with permission.³⁹ Copyright 2020, Elsevier Publishing Group. (h) Illustration of the fluorescent coding by fiber parallel arrangement of fibers spun with multiple nozzles in microfluidic spinning. Reproduced with permission.¹⁰ Copyright 2018, American Chemistry Society. (i and j) SEM images of SiO₂ particles ordered on a fiber surface. Reproduced with permission.⁴⁷ Copyright 2019, Elsevier Publishing Group.

textiles.³⁹ Owing to the versatile designs of microfluidic chips, multi-nozzle spinning chips were used to prepare parallel oriented fibers (Fig. 6h).¹⁰ Different fluorescent spinning solutions were used to fabricate aligned fluorescent microfibers with various colours, which could be used for versatile encoding of smart and wearable textiles.

3.4.2 Stacking density. The stacking density of the basic units, such as the nanoparticle distribution on the fiber surface or inside the fiber, is an important characteristic. For example, the packing density of nanoparticles on the fiber surface determines the spacing between the nanoparticles, which can be used to achieve different photonic crystal structures, where the apparent colour depends on the particle

spacing. As shown in Fig. 6i and j, when SiO₂ colloids were spun with viscous PVP ethanol solution and PAM by microfluidic spinning, the SiO₂ colloids were assembled into a photonic crystal structure on the fiber surface with a certain stacking density after removing the PVP.⁴⁷ The distance between the SiO₂ colloids changed in response to changes in the environmental humidity, indicating its potential for environment humidity detection or human respiratory monitoring applications.

3.4.3 Interaction. Physical and chemical interactions, such as adhesion, entanglement, and friction between the basic fiber units, depend on their morphology. These interactions allow the fibers to be twisted,³³ wrapped,^{27,119,120} or knotted⁸ together to form yarns, which are further woven,^{26,120} knitted,^{121,122} or braided¹²³ into fabrics. Two simultaneously spun fibers were twisted into a yarn (Fig. 7a) using post-spinning twisting devices, which enabled bonding interactions between the fibers, resulting in a higher yarn toughness compared with the original yarn (Fig. 7b).¹ The friction between the fibers enabled them to be knotted (Fig. 7c), and/or formed into regularly arranged fabrics (Fig. 7d and e). Li *et al.* fabricated self-healing supramolecular hydrogel fibers based on host-guest interactions by the microfluidic spinning technique, which was further used as a microreactor for construction of inter-fiber knot structures (Fig. 7f).⁴⁰ Mu *et al.* fabricated aligned warp and weft yarns with an ordered arrangement, where

chemical reactions between fluorescein and amine solutions occurred at the contact points of the microarrays (Fig. 7g).⁴⁹

The orientation, stacking density, and interactions between the multiscale basic units play a critical role in determining the fiber properties. Therefore, by tailoring the fiber structure during or after spinning, intelligent fiber devices with adjustable performance can be achieved.

4. Intelligent fiber devices

Previous sections showed that the tuneable microfluidic process can produce fibers with a small diameter, large specific surface area, and ordered surface structures. Such fiber materials are suitable for use in various devices, such as those for water collection, luminous applications, and tissue engineering, *etc.*

4.1 Water collection

Using biomimetic structures inspired by spider silk, researchers revealed that the surface structure and the knot morphology of the natural fiber have a direct effect on the water collection ability.^{3,112} Due to the superior control of the fiber shape characteristics provided by microfluidic spinning, knotted fibers prepared by this method are widely used in water collection.^{3,12,112,124} By adjusting the flow rate of the knot emulsification process by a novel microfluidic strategy, the size and distance of spindle knots on the microfibers

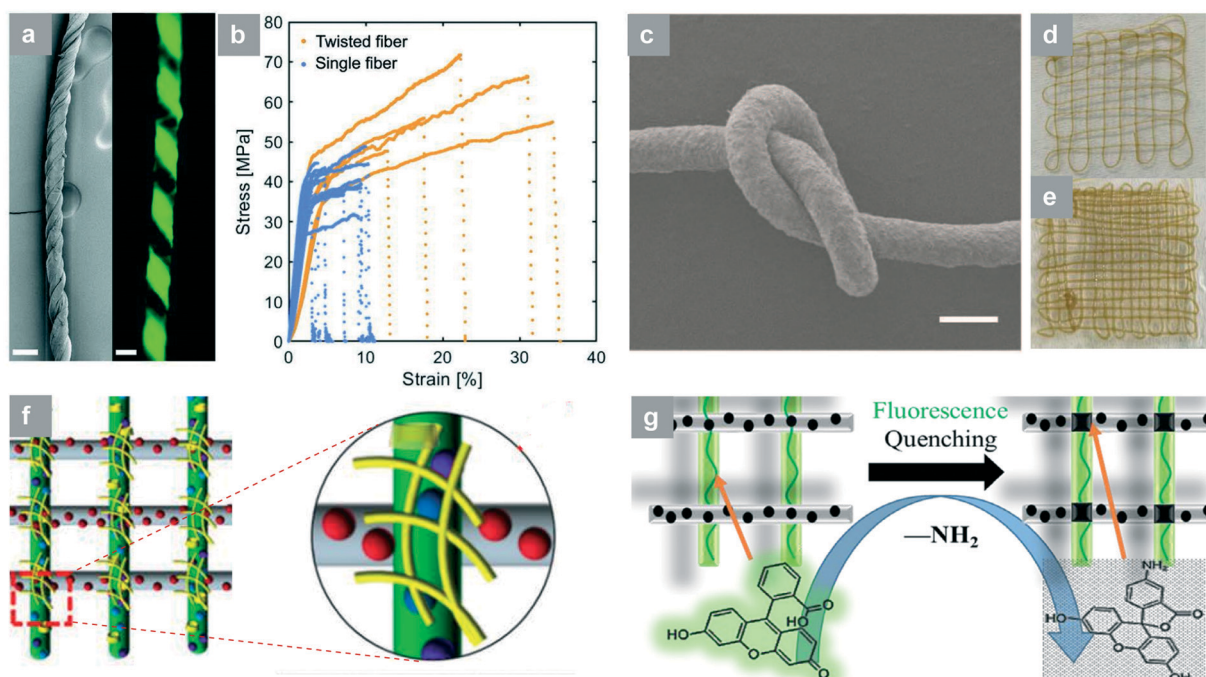


Fig. 7 Interactions between microfluidic spun fibers. (a) SEM and fluorescence images of twisted fibers. Reproduced with permission.¹ Copyright 2020, Wiley-VCH. (b) Stress-strain curve for the twisted yarn and single fiber shown in (a). Reproduced with permission.¹ Copyright 2020, Wiley-VCH. (c) A tightly knotted fiber.⁸ Copyright 2018, Wiley-VCH. (d and e) Fabric-like structures formed by 3D microfluidic printing technology. Reproduced with permission.¹⁶ Copyright 2020, American Chemistry Society. Schematics of (f) microreactors at fiber-fiber junctions⁴⁰ and (g) the corresponding under fluorescence reaction. Reproduced with permission.⁴⁹ Copyright 2017, Elsevier Publishing Group.

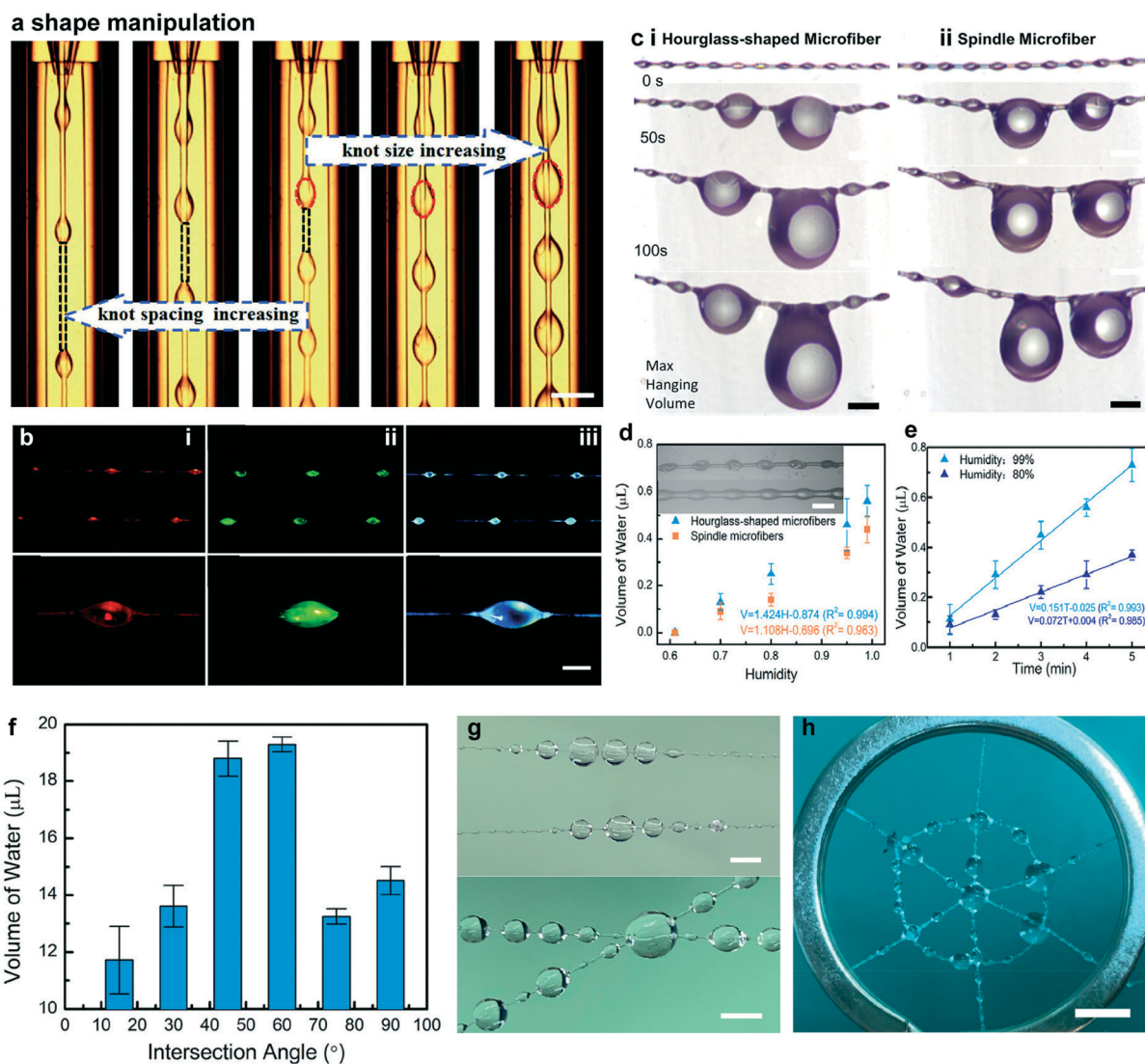


Fig. 8 The application of knotted microfluidic spun fibers for water collection. (a) Real-time microscopy images of the microfiber generation with controllable knot spacing and size. Reproduced with permission.³ Copyright 2017, Wiley-VCH. (b) Microscopy images of the microfibers with stable structural colours on spindle knots. The diameters of the PS nanoparticles were (i) 200 nm, (ii) 240 nm, and (iii) 280 nm, which resulted in red, green, and blue colours, respectively. Reproduced with permission.³ Copyright 2017, Wiley-VCH. (c) Comparison of the water collection capability of microfibers with hourglass-shaped or spindle-shaped knots and their corresponding (d) dehumidified volume and (e) relationship between the dehumidified volume and the hourglass-shaped microfiber length when the humidity values are fixed at 80% and 99%. Reproduced with permission.¹² Copyright 2020, American Chemistry Society. (f) The effect of the intersectional angle on the collected water volume. Reproduced with permission.¹² Copyright 2020, American Chemistry Society. (g) Photographs comparing the water collection of knotted fibers with or without an intersection angle. (h) Image of the spider-web-like network with hourglass-shaped microfibers for water collection. Reproduced with permission.¹² Copyright 2020, American Chemistry Society.

were precisely controlled (Fig. 8a). The specific knot structure provided by microfluidic spinning and the wettability of the microfibers enabled the droplets with nanoparticles being elongated along the fiber surface to generate spindle-shaped knots. By using different sized PS nanoparticles, microfibers with spindle knots can exhibit different colours (Fig. 8b).

To enhance the water-collection performance of the fibers, a bio-inspired microfiber with hourglass-shaped knots was fabricated by taking advantage of a non-solvent-induced phase separation process.¹² By manipulating the oil core spillage and the fluid flow configuration, hourglass-shaped

microfibers were obtained with various morphologies and densities. Compared with spindle microfibers, the prepared hourglass-shaped ones had enhanced water-collection volume (Fig. 8c). The water droplet volume collected on the hourglass-shaped knots increased almost linearly with the collection time, which was 1.64 times larger than that on the spindle knot domain (Fig. 8d). The dehumidified volume increased proportionately with increasing fiber length (Fig. 8e). The intersectional angle between the two microfibers also affected the water collection volume (Fig. 8f). Because of the difference in the liquid/vapour

interfacial tension between the two droplet ends, the droplets on each microfiber were orderly transported to the intersection. The water collection volume of fibers with a 60° intersectional angle was higher than that of two parallel fibers (Fig. 8g). The study proposed a biomimetic spider web design for environmental dehumidification and water collection (Fig. 8h). Intelligent fiber with water-collection capacity can be used in environmental dehumidification, directional droplet transportation, and water harvesting,

which may provide a novel method for people living in areas where fresh water is not available.

4.2 Encoded and luminous fibers

By combining the microfluidic technology with the wet-spinning process, microfluidic spinning can be used to generate fibers incorporating spherical materials, such as polymer microspheres, hydrophobic microdroplets or

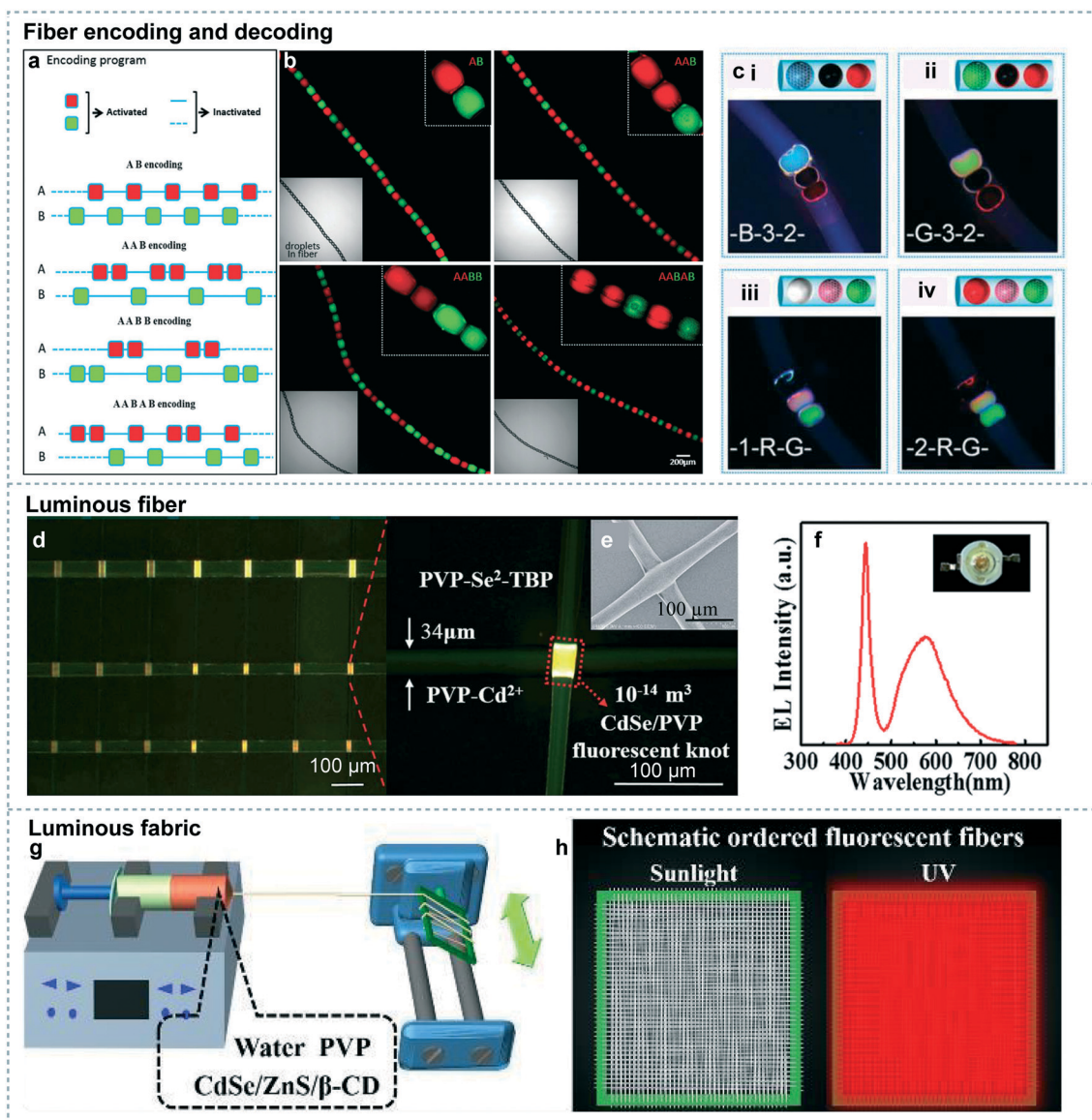


Fig. 9 The application of luminous microfluidic spun fibers. (a) Schematic description of color encoding by controlled deposition of fluorescent droplets during processing. Reproduced with permission.¹⁷ Copyright 2014, Wiley-VCH. (b) Confocal images of a dehydrated CaA fiber encoded using red and green droplets. Reproduced with permission.¹⁷ Copyright 2014, WILEY-VCH. (c) Color-encoded microfibers with a combination of colloidal crystal microdots and dye-filled microdots. Reproduced with permission.¹¹ Copyright 2019, Royal Society of Chemistry. (d) Fluorescence microscopy images of CdSe QD arrays, and an SEM image of the microfiber knot (e).⁵⁰ Copyright 2015, Royal Society of Chemistry. (f) Emission spectrum of a WLED based on CdSe/PVP powders operated at 350 mA. Inset: Photograph of the WLED under daylight. Reproduced with permission.⁵⁰ Copyright 2015, Royal Society of Chemistry. (g) Schematic of the microfluidic spinning process used to produce the PVP fiber containing CdSe/ZnS/β-Cd QDs. (h) Fluorescent fabrics prepared using these fibers under sunlight and UV irradiation. Reproduced with permission.⁶⁶ Copyright 2019, Royal Society of Chemistry.

multicellular spheroids with controllable order. Therefore, programmable equipment can be used to produce fibers embedded with different spherical materials in typical sequences for coding and decoding applications. Yu *et al.* encoded CaA microfibers with *n*-hexadecane droplets combined with fluorescein and rhodamine B (Fig. 9a) to form four encoded patterns (-A-B-, -A-A-B-, -A-A-B-B-, and -A-A-BA-B) (Fig. 9b).¹²⁵ In addition, in the microfibers, dye microdots and colloidal crystals of tuneable size, spacing, number, and sequence were orthogonally and simultaneously embedded to produce a designed pattern (Fig. 9c).¹¹

In addition, microfluidic spinning has been widely applied to produce fluorescent fibers, some of which were further formed into fabrics.^{50,66,96,126–128} Microfluidic spinning was

used to produce 1D microfibers, where inter-fiber junctions and knots were then added as the microreactors, to synthesize fluorescent CdSe hybrid quantum dots (QDs) *in situ via* a solid–solid contact reaction.¹¹⁵ The CdSe hybrid fibers were further ground into powder and applied as the phosphor to prepare white light-emitting diodes (WLED) (Fig. 9d and e) with obvious emission peaks (Fig. 9f). Red- and yellow-emissive CdSe/ZnS/ β -CD QDs with photoluminescence quantum yields (80–82%) were produced, and then incorporated in PVP fibers using a microfluidic method (Fig. 9g).⁶⁶ These fibers were then used to prepare highly fluorescent fabrics with ordered alignment *via* microfluidic spinning (Fig. 9h), with possible applications in flexible displays or wearable detectors. Colour-coded

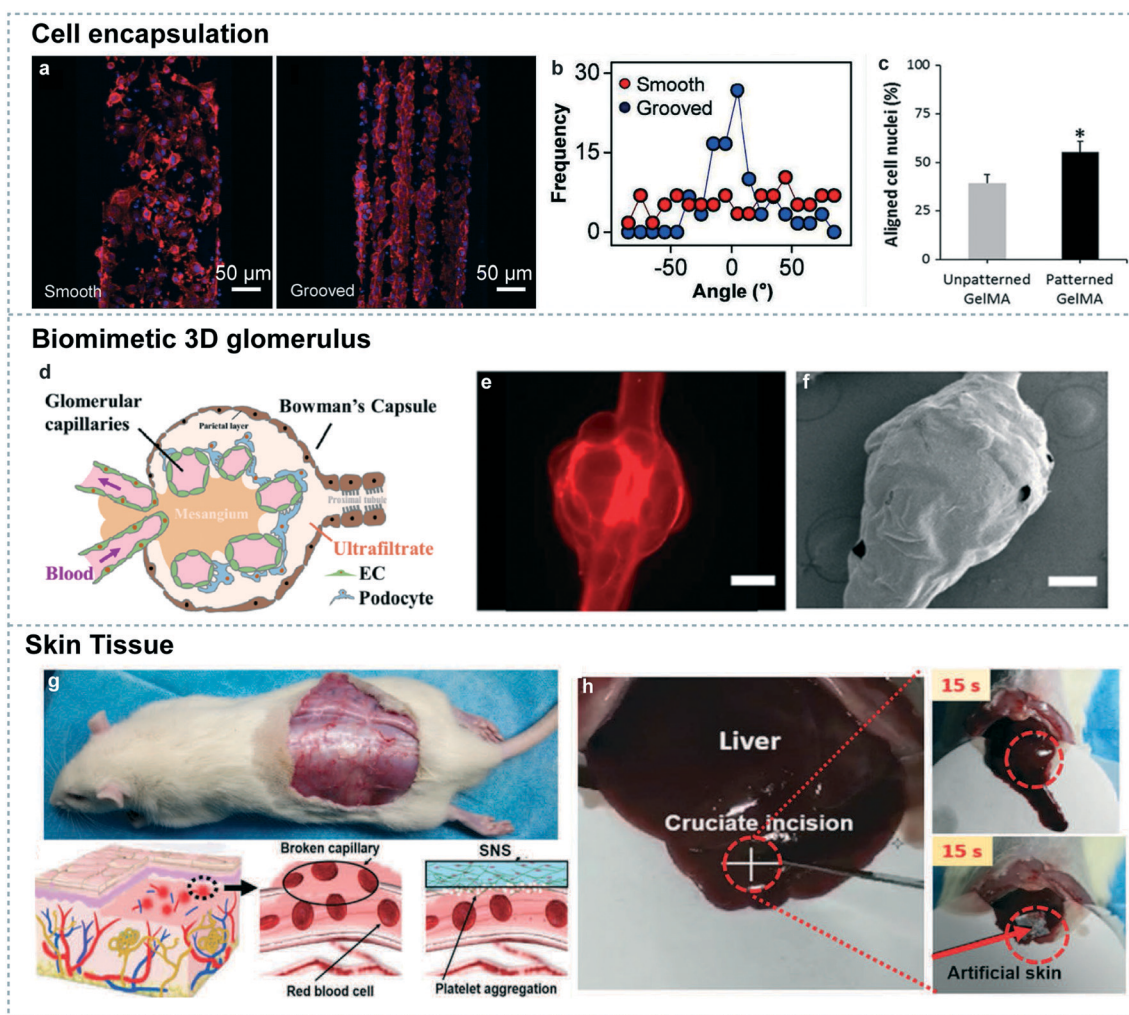


Fig. 10 Application of microfluidic spun fibers in tissue engineering. Cell encapsulation on smooth and grooved fibers: (a) fluorescence microscopy images; (b) quantification of the neurite orientation. Reproduced with permission.²⁰ Copyright 2012, Wiley-VCH. (c) Quantification of the aligned cell nuclei on unpatterned and patterned GelMA fibers. Reproduced with permission.²² Copyright 2018, Springer Nature. (d) Schematic diagram, (e) fluorescence image, and (f) SEM image of the microconvex topography of the scaffold surface of an h-FIBER. Reproduced with permission.²⁴ Copyright 2020, American Chemistry Society. (g) Photograph of a wounded mouse and a corresponding schematic of the haemostasis of broken blood vessels on the wound surface being treated using a biodegradable nanofiber scaffold. (h) Photographs of a bleeding rat liver model showing: (left) the rat liver, (top right) the rat liver bleeding, and (bottom right) haemostasis by a sealant-loaded nanofiber scaffold. Reproduced with permission.³⁸ Copyright 2020, Wiley-VCH.

microfibers have a wide range of applications in the food industry, anti-counterfeiting, and bioassay fields, among others.

4.3 Tissue engineering

In addition to the good shape control, microfluidic spinning methods are superior to conventional methods for processing sensitive biological materials as the fluid is exposed to ambient conditions (no high voltage, temperature, or stress), which are suitable for tissue engineering.⁶² Therefore, such methods are widely used in the fields of cell culture,^{22,129–135} drug release,^{136,137} biomimetic tissue design,²⁴ and skin tissues.^{38,138} Shape characteristics, such as the fiber morphology and surface structure, play an important role in cell encapsulation. To control the organization of cells, Kang *et al.* fabricated cell-aligning scaffolds by microfluidic spinning, and studied the cell encapsulation and alignment along the alginate microfibers with either smooth or grooved microstructures.²⁰ As shown in Fig. 10a, on the grooved fiber surface, many neuron cells adhered to the ridges of the grooves. On the contrary, most of the neuron cells on the smooth fibers migrated to the edges and gathered to form networks across the fibers. They further calculated the alignment angles between the fiber axis direction and the neurites on the grooved fibers. For the grooved fibers, most neurites were well ordered along the fiber because the alignment angle was narrowly distributed around 0°, whereas neurites were randomly orientated as the alignment angle distributed on the smooth fibers was broad (Fig. 10b).

Ebrahimi *et al.* fabricated microfluidic spun gelatin methacryloyl (GelMA) fibers with surface grooves and showed that the C2C12 myoblast alignment was significantly enhanced compared to that of the equivalent smooth fibers (Fig. 10c).²²

The shape characteristics control provided by microfluidic spinning also provides an effective method for producing biomimetic 3D glomeruli (Fig. 10d–f).²⁴ A microfluidic-extruded topographic hollow fiber (h-FIBER) was produced, which consisted of a single vessel-like perfusable tubular channel for endothelial cell culture, with a glomerulus-like knot of microconvex topography on the surface for podocyte cell culture. Compared to the tube regions, the knot regions of the h-FIBER showed enhanced podocyte interdigitation. Based on the fiber structure, a functional filtration barrier was demonstrated. In addition, nanofiber-based scaffolds fabricated by microfluidic spinning have been applied in skin tissue engineering. A biodegradable sealant-loaded nanofiber scaffold was fabricated by microfluidic blow-spinning, which helped rapidly repair acute tissue damage (Fig. 10g), such as vascular and hepatic haemorrhage (Fig. 10h), and also promote repair of large abdominal wall defects, angiogenesis and wound tissue regeneration.³⁸ This strategy provides a facile method to regenerate robust skin over a large area.

Microfluidic spinning has proved to be a superior method for producing fibers for tissue engineering applications, as

the mild spinning conditions are suitable for biological materials, which is critical for cell culture, drug release, biomimetic tissue design, and skin tissue applications. In addition, such fibers can easily be woven into various complex shapes, which promotes the future fabrication of artificial *in-vivo* blood vessels and/or organs by weaving the microfluidic spun fibers.

4.4 Fiber sensors and actuators

Changes in the fiber shape in response to external stimuli (*e.g.*, bending, strain, and humidity) can be used to provide functionality in various sensor applications. For example, a simple helical microfiber was attached to an elastic GelMA hydrogel film, and used as a mechanical sensor for cardiomyocytes.¹³ By immobilizing the two ends of the microfiber–film composite, the helical microfiber underwent cycles of elongation and contraction in response to the beating of the cardiomyocytes (Fig. 11a). Wei *et al.* fabricated polyacrylamide (PAA)/alginate hydrogel microfibers and printed them in a web-like structure.²⁹ After wrapping the web-like fabric around the volunteer's elbow, clear changes in the resistivity were detected during repeated bending and stretching of the elbow, which accurately conformed to the real-time physiological behaviour (Fig. 11b). Colloidal photonic crystals were mixed with polymers and assembled into 1D fibers by microfluidic spinning to produce fibers with different colours. Humidity sensing based on the particle spacing is possible with such fibers. Humidity-sensitive polyacrylamide (PAM)/SiO₂ composite photonic crystal fibers were fabricated, where the PAM was successfully introduced into the fiber and filled the voids between SiO₂ particles (Fig. 11c).⁴⁷ The colour of the fiber changed from blue to yellow, orange, and red consecutively with increasing relative humidity (25–100%) (Fig. 11d) due to the PAM absorbing water and swelling, resulting in increasing distance between the SiO₂ particles. The corresponding shifts in the reflectance spectra with changing humidity (Fig. 11e) showed an obvious and quick humidity response and recovery.

Zhou *et al.* fabricated continuous bilayer hydrogel fibers with one layer of CaA hydrogel and another layer of CaA/graphene oxide (GO)/linear poly(*N*-isopropylacrylamide) (PNIPAM) by microfluidic spinning (Fig. 12a).¹⁵ The bilayer hydrogel fibers had the specific porous internal structure of a semi-interpenetrating polymer network (semi-IPN), where the pore size decreased with increasing GO content. The bilayer hydrogel fibers bent in response to changes in the temperature and near-infrared (NIR) light exposure (Fig. 12b). Using a coaxial microfluidic apparatus, thermoresponsive semi-IPN hydrogel microfibers with fast response and high elasticity were developed (Fig. 12c).¹⁹ Film actuators based on the hydrogel microfibers were fabricated, which also showed fast shape transformations in response to temperature changes (Fig. 12d).

Microfluidic-spun helical-shaped fibers were used as flexible actuators for rotating and crawling movements.¹³

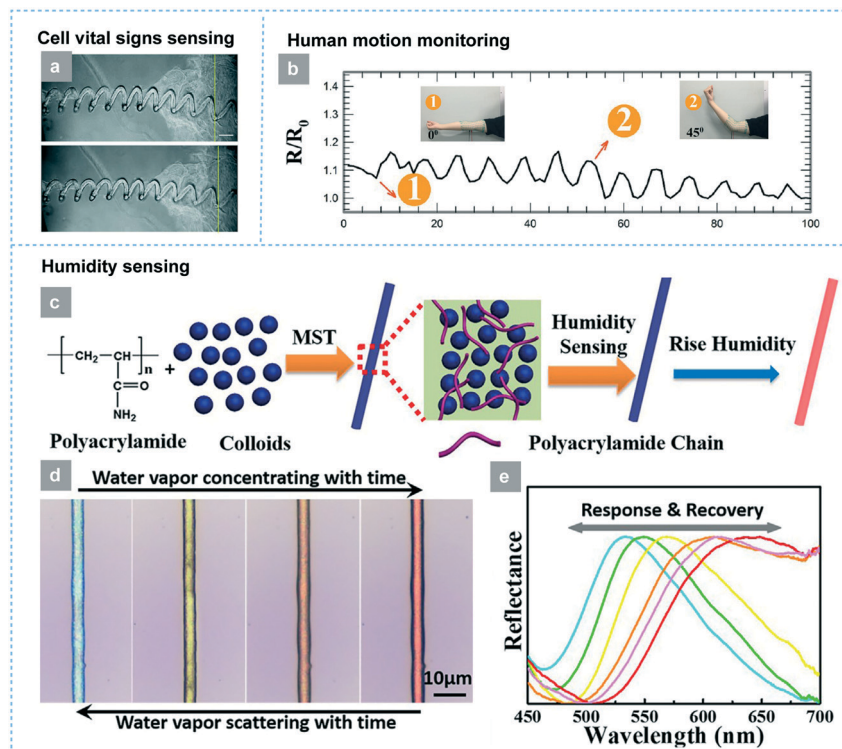


Fig. 11 The application of microfluidic spun fibers in flexible sensors. (a) Application of helical fibers to sense the beating activity of cardiomyocytes based on the vibration bending. Reproduced with permission.¹³ Copyright 2017, Wiley-VCH. (b) Human motion using a microfluidic-fiber woven fabric with the elbow subjected to repeated bending. Reproduced with permission.²⁹ Copyright 2018, American Chemistry Society. (c) Schematic diagram and (d) photographs of humidity sensing *via* color changes of a pam composite fiber when water molecules are absorbed and released, and the (e) corresponding reflectance spectra at different humidity values. Reproduced with permission.⁴⁷ Copyright 2019, Elsevier Publishing Group.

Helical micromotors with different components were fabricated using a microfluidic spinning and spiralling system (Fig. 12e).⁵ Based on the functional nanoparticle encapsulation, the helical micromotors were able to move by magnetically actuated rotation or corkscrew motions, as well as *via* a chemically driven catalytic reaction (Fig. 12f). The helical micromotor showed obvious movements when they are exposed to magnetic fields in different directions (Fig. 12g). To achieve enhanced rotation-based locomotion, Tang *et al.* developed a hollowed helical magnetic hybrid microswimmer taking advantage of microfluidic template synthesis and biosilicification (Fig. 12h).⁵⁵ The hybrid microswimmers were fabricated by synthesizing helical CaA fibers containing Fe_3O_4 nanoparticles with a microfluidic method, followed by biosilicification and controlled dicing. These microswimmers were able to transport several ethoxylated trimethylolpropane triacrylate (poly-ETPTA) microspheres through tubes containing deionized water (Fig. 12i–k).

Fiber sensors and actuators are an important part of smart textiles, which are expected to bring traditional textiles into a new era with monitoring and self-adaptive functionalities. Microfluidic spinning is proving to be a desirable platform for fabricating fibers with sensing and actuating capability. However, most of the sensing functionalities are still focused

on strain or humidity detection, while the actuators are mainly operated by temperature or NIR irradiation. Textiles are the “second skin” of human beings, and the development of a wider range of fiber sensors that can be integrated into such textiles for monitoring *e.g.*, the body and environmental temperature, as well as the glucose, calcium, and potassium ions in human sweat could provide many benefits in healthcare.

4.5 Fiber energy devices

The microfluidic spinning method has been widely used for the preparation of fiber supercapacitors (SCs)^{8,14,18,41,56,127,139,140} as it provides one-step fabrication by taking advantage of the multi-channel co-flow strategy. Inspired by the hierarchical structure of natural silk fiber, multicomponent SC microfibers were fabricated with one or two separated CNTs in the core and PU in the shell (Fig. 13a).¹⁸ Because of the encapsulation of the CNTs with an insulating material, the microfibers showed capacitive behaviour when a voltage was applied. When the CNT fiber suffers from a certain voltage, polarization would occur on both sides of the microfiber. Compared with the single-CNT core, microfibers with double CNT cores had higher capacitance owing to the increased number of charges stored in the CNTs, as indicated by the equations used to calculate the

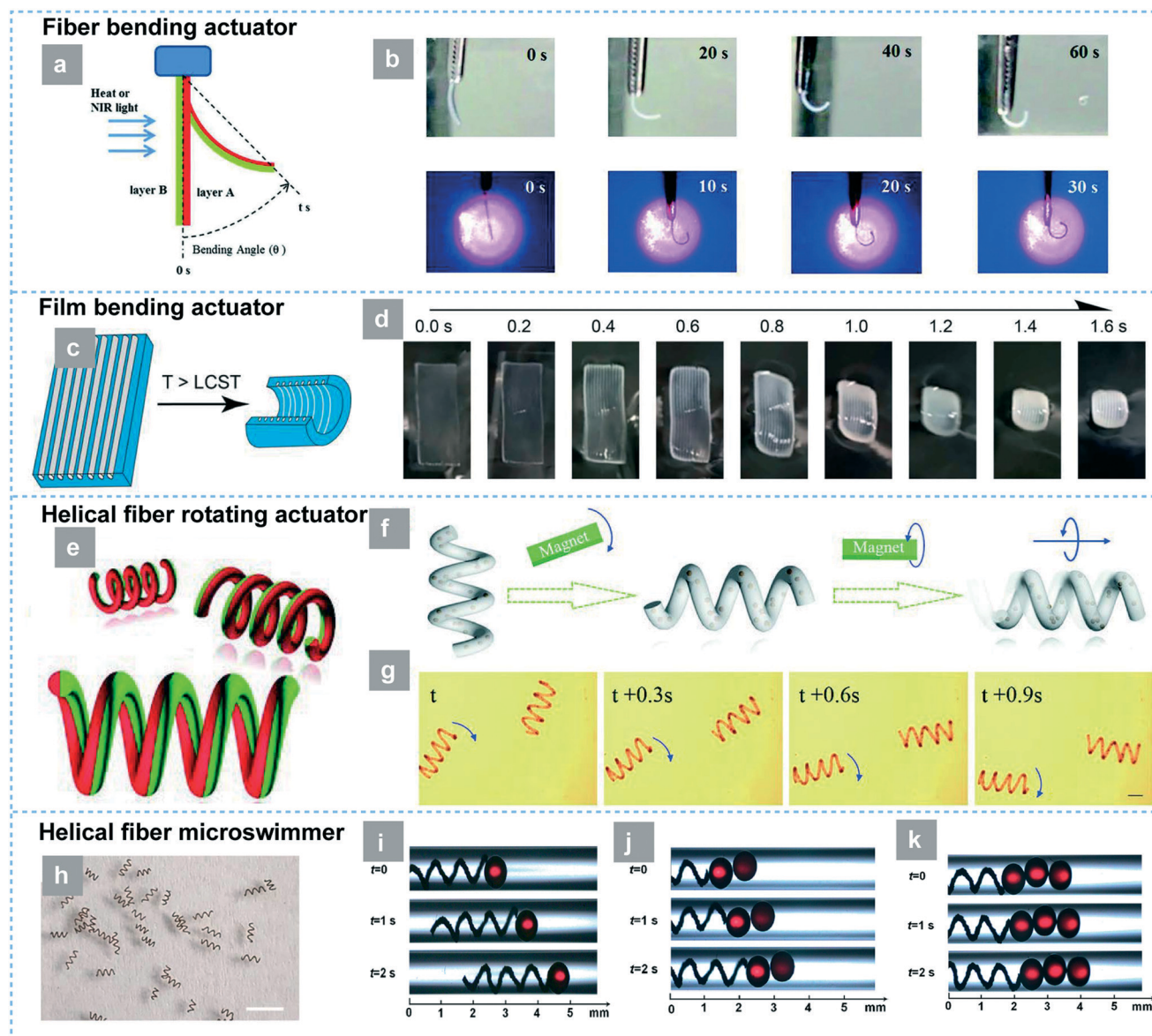


Fig. 12 Application of microfluidic spun fibers in flexible actuators. (a and b) A bilateral fiber in a bending actuator.¹⁵ Copyright 2019, European Polymer Federation. (c and d) Schematic of the temperature-stimulated folding of a hydrogel film and the experimental results show the shape transformation. Reproduced with permission.¹⁹ Copyright 2017, American Chemistry Society. Illustrations of (e) bilayer helical micromotors responding to (f) clockwise rotary and 3D rotating magnetic fields, and (g) their movement under magnetic fields with different directions. Reproduced with permission.⁵ Copyright 2017, Wiley-VCH. (h) Microscopy image of the magnetic helical CaA microfibers. (i–k) Optical images of magnetic hybrid microswimmers for the transportation of one, two, or three poly-ETPTA microspheres in deionized water. Reproduced with permission.⁵⁵ Copyright 2018, American chemistry society.

capacitance in Fig. 13b and c. The high mechanical flexibility and energy-storage ability of the SC microfiber enabled it to be weaved into a Chinese-knot shape, which was used to power LEDs (Fig. 13d). The prepared CNT microfibers had good stability, flexibility and long-term cyclic energy storage ability during various electrochemical tests.

The scalable microfluidic blow-spinning method can also be used to fabricate nanofiber-based flexible SC electrodes with excellent mechanical strength. Using hierarchical metal–organic framework/graphene/CNT hybrids, Cheng *et al.* fabricated a SC with high specific capacitance (472 F cm^{-3}), large volumetric

energy density ($147.5 \text{ mW h cm}^{-3}$) and deformation-stable energy supply.⁵⁶ The fiber-based SCs showed high bending stability, with no obvious capacitance (Fig. 13e). Under twisting deformation, the capacitance of the flexible SC was even increased (Fig. 13f). A typical solar–electrochemical self-powered system that combined a solar cell with a wearable SC was demonstrated (Fig. 13g). The photons were converted into electricity by the solar cell (energy harvesting unit) under simulated solar irradiation, where the energy was then stored as electrochemical energy by the wearable supercapacitor. After continuous illumination for 60 s, the self-powered device stored

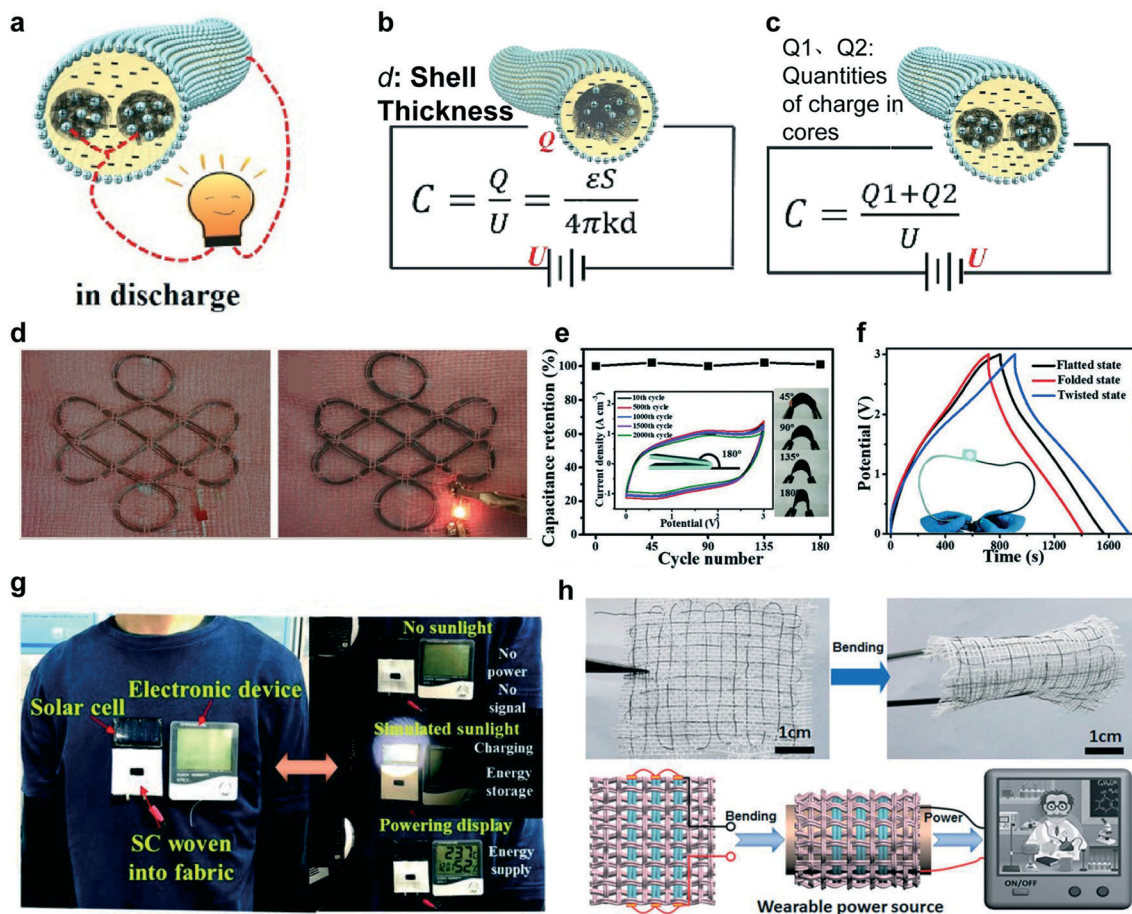


Fig. 13 Supercapacitor applications of microfluidic spun fibers. Schematic diagrams of a (a) microfluidic spun fiber SC and the capacitance test setup for microfibers with (b) one or (c) two CNT cores. Reproduced with permission.¹⁸ Copyright 2018, Elsevier Publishing Group. (d) Photographs of microfiber SCs in the form of a Chinese knot before and during charging. Reproduced with permission.¹⁸ Copyright 2018, Elsevier Publishing Group. (e) Capacitance retentions of SCs subjected to different bending angles. (f) Galvanostatic charge/discharge curves of a SC when flat, twisted, and folded. Reproduced with permission.⁵⁶ Copyright 2018, Wiley-VCH. (g) Optical images of flexible SCs for solar cell harvesting, storing solar energy, and display powering. Reproduced with permission.⁵⁶ Copyright 2018, Wiley-VCH. (h) Photographs and schematics of a long PNA/G composite fiber woven into a cotton fabric, which could withstand bending deformations. Reproduced with permission.¹⁴ Copyright 2018, Royal Society of Chemistry.

enough energy to make a display light up. Wu *et al.* fabricated a micro SC based on microfluidic technology with a highly electrochemically active polyaniline nanorod array (PNA) shell with a highly conductive graphene core.¹⁴ This core-shell structure produced a micro-SC fiber with large pseudocapacitance, excellent bending durability and high cycling stability. The SC fiber was woven into a cotton fabric for wearable electronics, which was able to withstand mechanical bending (Fig. 13h). Microfluidic methods have been demonstrated for controlled production of fiber SCs, which are expected to revolutionize future wearable electronics.

5. Future perspectives and concluding remarks

This review discussed the development of newly emerged microfluidic methods for fabricating intelligent fiber devices according to microfluidic spinning platforms, resulting in

fiber shape characteristics and their applications. There is a large body of literature related to the shape manipulation of fibers using microfluidic fabrication approaches, although the importance of the shape characteristics has often been secondary to the quality characteristics. Therefore, this review discussed the fiber shape characteristics and clearly highlighted the importance of controlling these factors during microfluidic spinning to tailor the fiber performance for specific applications. We emphasized the importance of the fiber dimensions for controlling its specific surface area, which directly affects the absorption of moisture and dyes, mechanical performance, and appearance of the fibrous materials. We classified and summarized the different morphologies of microfluidic spun fibers and discussed the important role of the fiber surface in determining its interaction with other fibers and surfaces. The microfluidic method is advantageous for producing fibers with a good mechanical performance, enabled by the alignment of

nanofibrils by the shearing flows in the fluid channel. A particularly interesting application is the encoding of the fibers by controlled patterning. Finally, intelligent fiber devices based on microfluidic fibers were discussed, which take advantage of the *e.g.*, water collection, luminosity, encoding, biomimetic, and energy storage properties of the fibers enabled by the microfluidic technology.

It is clear that microfluidic approaches provide a powerful platform for micro/nanoscale fiber shape manipulation, which is enabling researchers in the materials science and textile fields to take advantage of the wide range of shape characteristics. Further research and development on microfluidic spinning should be focused on increasing the diversity of microfluidic chip designs, and strategies for controlling the fiber diameter and morphology, to enable the use of a wider range of raw materials. More microfluidic technologies for fiber spinning should be developed considering the various chip-design and hydromechanics technologies to realize fiber shape manipulation. In addition to the well-known microfluidic fiber formation technologies based on laminar flow, further microfluidic technologies could be developed for intelligent fiber fabrication in future research, such as the use of patterned nanochannels for functional nanofibril or nanoparticle self-assembly, or stretching and orienting of the nanofibrils by liquid surface tension to achieve additional functionalities of the intelligent fiber devices.

In addition, although microfluidics has proven to be an excellent platform for the development of biomimetic silk fibers, it is still difficult to fabricate systems similar to the glands of spiders or silkworms and control the protein generation. Hence, in most cases, the mechanical performances of the regenerated fibers are still not comparable with the natural ones. In the future, more diverse microfluidic chips could be developed for fiber spinning to achieve better performance and high strength. Reducing the fiber to the nanoscale by decreasing the chip dimensions or increasing the shearing effect is expected to enhance their performance. In addition, mass production still faces many challenges because of the complexity of the microfluidic chip design and the highly precise operating conditions required. Hence, further research focused on upscaling the chip designs for mass production is necessary. Textile engineering research should also focus on the directed collection of the microfluidic spun fibers and methods for weaving them into 2D or 3D fabrics by programmable nozzle movement, which is expected to diversify the application of microfluidic micro/nanoscale fibers.

The broad application of functional microfluidic fibers has been demonstrated recently. Intelligent fiber devices are only the basic units of smart textiles, and further study of methods for twisting intelligent fibers into yarns, and then producing smart fabrics is still lacking. Future smart textile research should consider the conformity with human skin, fabric style, and clothing comfort, to promote wider application of smart textiles and bring

traditional textiles into a new era of monitoring and self-adaptive functionality. Further applications, such as biosensors and humidity actuators, fiber electronics, and fiber photonic devices, could also be developed using microfluidic spinning. If the microfluidic spun fibers are strong enough, they can be woven into artificial *in vivo* blood vessels and/or organs in the future, which will broaden their applications in tissue engineering. In addition, fibers with energy harvesting and storage functionality can enable devices with closed-loop energy systems for smart textiles.

In conclusion, we believe that microfluidic spinning is an excellent method for producing various advanced fibers with increasingly tuneable and programmable morphology, smaller fiber size, and complex surface structures, which will endow the fibers with desirable performance and contribute to substantial progress in the next-generation smart textile industries.

Author contributions

T. K. and R. W. conceived the idea and wrote the manuscript.

Conflicts of interest

There are no conflicts to declare.

Acknowledgements

This work was supported by a National Research Foundation of Korea (NRF) grant funded by the Korean government (MSIT) (NRF-2020R1A2C3003344 and NRF-2020R1A4A2002728).

Notes and references

- 1 A. Kamada, A. Levin, Z. Toprakcioglu, Y. Shen, V. Lutz-Bueno, K. N. Baumann, P. Mohammadi, M. B. Linder, R. Mezzenga and T. P. J. Knowles, *Small*, 2020, **16**, 1904190.
- 2 L. Lu, S. N. Fan, Q. Q. Niu, Q. F. Peng, L. H. Geng, G. S. Yang, H. L. Shao, B. S. Hsiao and Y. P. Zhang, *ACS Sustainable Chem. Eng.*, 2019, **7**, 14765–14774.
- 3 L. R. Shang, F. F. Fu, Y. Cheng, Y. R. Yu, J. Wang, Z. Z. Gu and Y. J. Zhao, *Small*, 2017, **13**, 1600286.
- 4 Y. Cheng, Y. R. Yu, F. F. Fu, J. Wang, L. R. Shang, Z. Z. Gu and Y. J. Zhao, *ACS Appl. Mater. Interfaces*, 2016, **8**, 1080–1086.
- 5 Y. R. Yu, L. R. Shang, W. Gao, Z. Zhao, H. Wang and Y. J. Zhao, *Angew. Chem., Int. Ed.*, 2017, **56**, 12127–12131.
- 6 Y. R. Yu, L. R. Shang, J. H. Guo, J. Wang and Y. J. Zhao, *Nat. Protoc.*, 2018, **13**, 2557–2579.
- 7 G. L. Zhou, G. Yang, X. L. Li, B. Y. Chen, J. Fan, X. Hou and S. B. Zhou, *ACS Appl. Mater. Interfaces*, 2018, **10**, 14276–14280.
- 8 Y.-L. Tong, B. Xu, X.-F. Du, H.-Y. Cheng, C.-F. Wang, G. Wu and S. Chen, *Macromol. Mater. Eng.*, 2018, **303**, 1700664.

- 9 S. K. Chae, E. Kang, A. Khademhosseini and S. H. Lee, *Adv. Mater.*, 2013, **25**, 3071–3078.
- 10 T. T. Cui, Z. J. Zhu, R. Cheng, Y. L. Tong, G. Peng, C. F. Wang and S. Chen, *ACS Appl. Mater. Interfaces*, 2018, **10**, 30785–30793.
- 11 Z. J. Meng, J. Zhang, X. Deng, J. Liu, Z. Y. Yu and C. Abell, *Mater. Horiz.*, 2019, **6**, 1938–1943.
- 12 R. Shi, Y. Tian, P. G. Zhu, X. Tang, X. W. Tian, C. M. Zhou and L. Q. Wang, *ACS Appl. Mater. Interfaces*, 2020, **12**, 29747–29756.
- 13 Y. Yu, F. Fu, L. Shang, Y. Cheng, Z. Gu and Y. Zhao, *Adv. Mater.*, 2017, **29**, 1605765.
- 14 X. J. Wu, G. Wu, P. F. Tan, H. Y. Cheng, R. Hong, F. X. Wang and S. Chen, *J. Mater. Chem. A*, 2018, **6**, 8940–8946.
- 15 M. L. Zhou, J. H. Gong and J. H. Ma, *e-Polym.*, 2019, **19**, 215–224.
- 16 H. B. Qing, Y. Ji, W. F. Li, G. X. Zhao, Q. Z. Yang, X. H. Zhang, Z. T. Luo, T. J. Lu, G. R. Jin and F. Xu, *ACS Appl. Mater. Interfaces*, 2020, **12**, 2049–2058.
- 17 Y. Yu, H. Wen, J. Y. Ma, S. Lykkemark, H. Xu and J. H. Qin, *Adv. Mater.*, 2014, **26**, 2494–2499.
- 18 J. H. Guo, Y. R. Yu, L. Y. Sun, Z. H. Zhang, Y. J. Zhao, R. J. Chai and K. Q. Shi, *Chem. Eng. J.*, 2020, **397**, 125517.
- 19 Y. Liu, K. H. Zhang, J. H. Ma and G. J. Vancso, *ACS Appl. Mater. Interfaces*, 2017, **9**, 901–908.
- 20 E. Kang, Y. Y. Choi, S. K. Chae, J. H. Moon, J. Y. Chang and S. H. Lee, *Adv. Mater.*, 2012, **24**, 4271–4277.
- 21 M. Hu, R. S. Deng, K. M. Schumacher, M. Kurisawa, H. Y. Ye, K. Purnamawati and J. Y. Ying, *Biomaterials*, 2010, **31**, 863–869.
- 22 M. Ebrahimi, S. Ostrovidov, S. Salehi, S. B. Kim, H. Bae and A. Khademhosseini, *J. Tissue Eng. Regen. Med.*, 2018, **12**, 2151–2163.
- 23 W. Yu and C. Chu, *Textile Materials*, ChinaTextile Press, 2019.
- 24 R. X. Xie, A. Korolj, C. Liu, X. Song, R. X. Z. Lu, B. Y. Zhang, A. Ramachandran, Q. L. Liang and M. Radisic, *ACS Cent. Sci.*, 2020, **6**, 903–912.
- 25 L. Ma, M. Zhou, R. Wu, A. Patil, H. Gong, S. Zhu, T. Wang, Y. Zhang, S. Shen, K. Dong, L. Yang, J. Wang, W. Guo and Z. L. Wang, *ACS Nano*, 2020, **14**, 4716–4726.
- 26 R. Wu, L. Ma, C. Hou, Z. Meng, W. Guo, W. Yu, R. Yu, F. Hu and X. Y. Liu, *Small*, 2019, e1901558, DOI: 10.1002/smll.201901558.
- 27 L. Y. Ma, R. H. Wu, A. Patil, S. H. Zhu, Z. H. Meng, H. Q. Meng, C. Hou, Y. F. Zhang, Q. Liu, R. Yu, J. Wang, N. B. Lin and X. Y. Liu, *Adv. Funct. Mater.*, 2019, **29**, 1904549.
- 28 Y. Srivastava, I. Loscertales, M. Marquez and T. Thorsen, *Microfluid. Nanofluid.*, 2008, **4**, 245–250.
- 29 S. Wei, G. Qu, G. Luo, Y. Huang, H. Zhang, X. Zhou, L. Wang, Z. Liu and T. Kong, *ACS Appl. Mater. Interfaces*, 2018, **10**, 11204–11212.
- 30 J. A. Matthews, G. E. Wnek, D. G. Simpson and G. L. Bowlin, *Biomacromolecules*, 2002, **3**, 232–238.
- 31 D. Zhang and J. Chang, *Adv. Mater.*, 2007, **19**, 3664–3667.
- 32 R. H. Wu, L. Y. Ma, A. Patil, C. Hou, S. H. Zhu, X. W. Fan, H. Z. Lin, W. D. Yu, W. X. Guo and X. Y. Liu, *ACS Appl. Mater. Interfaces*, 2019, **11**, 33336–33346.
- 33 L. Ma, Q. Liu, R. Wu, Z. Meng, A. Patil, R. Yu, Y. Yang, S. Zhu, X. Fan, C. Hou, Y. Li, W. Qiu, L. Huang, J. Wang, N. Lin, Y. Wan, J. Hu and X. Y. Liu, *Small*, 2020, **16**, e2000203.
- 34 Q. Liu, Z. Meng, R. Wu, L. Ma, W. Qiu, H. Zhang, S. Zhu, L. Kong, Z. Xu, A. Patil and X. Liu, *Fibers Polym.*, 2019, **20**, 2222–2226.
- 35 M. Costantini, C. Colosi, W. Swieszkowski and A. Barbetta, *Biofabrication*, 2019, **11**, 012001.
- 36 X. L. Zhang, C. Huang, Y. Zhao and X. Y. Jin, *J. Biomater. Sci., Polym. Ed.*, 2017, **28**, 1408–1425.
- 37 Y. Srivastava, M. Marquez and T. Thorsen, *Biomechanics*, 2009, **3**, 012801.
- 38 T. T. Cui, J. F. Yu, Q. Li, C. F. Wang, S. Chen, W. J. Li and G. F. Wang, *Adv. Mater.*, 2020, **32**, 2000982.
- 39 W. Zhang, C. Hou, Y. Li, Q. Zhang and H. Wang, *J. Colloid Interface Sci.*, 2020, **558**, 115–122.
- 40 Q. Li, Z. Xu, X. F. Du, X. Y. Du, H. Y. Cheng, G. Wu, C. F. Wang, Z. F. Cui and S. Chen, *Chem. Mater.*, 2018, **30**, 8822–8828.
- 41 G. Wu, P. Tan, X. Wu, L. Peng, H. Cheng, C.-F. Wang, W. Chen, Z. Yu and S. Chen, *Adv. Funct. Mater.*, 2017, **27**, 1702493.
- 42 C. Rong and B. Shen, *Chin. Phys. B*, 2018, **27**, 117502.
- 43 M. J. Sun, Y. P. Zhang, Y. M. Zhao, H. L. Shao and X. C. Hu, *J. Mater. Chem.*, 2012, **22**, 18372–18379.
- 44 I. Brazinsky, A. G. Williams and H. L. LaNieve, *Polym. Eng. Sci.*, 1975, **15**, 834–841.
- 45 M. Yamada, S. Sugaya, Y. Naganuma and M. Seki, *Soft Matter*, 2012, **8**, 3122–3130.
- 46 L. R. Shang, Y. T. Wang, Y. R. Yu, J. Wang, Z. Zhao, H. Xu and Y. J. Zhao, *J. Mater. Chem. A*, 2017, **5**, 15026–15030.
- 47 G. X. Li, H. X. Shen, Q. Li, Y. Tian, C. F. Wang and S. Chen, *Mater. Lett.*, 2019, **242**, 179–182.
- 48 Y. Srivastava, C. Rhodes, M. Marquez and T. Thorsen, *Microfluid. Nanofluid.*, 2008, **5**, 455–458.
- 49 R.-J. Mu, Y. Ni, L. Wang, Y. Yuan, Z. Yan, J. Pang and S. Chen, *Mater. Lett.*, 2017, **196**, 410–413.
- 50 W. Liu, Y. Zhang, C.-F. Wang and S. Chen, *RSC Adv.*, 2015, **5**, 107804–107810.
- 51 K. Yao, W. Li, K. Li, Q. Wu, Y. Gu, L. Zhao, Y. Zhang and X. Gao, *Macromol. Biosci.*, 2020, **20**, 1900395.
- 52 W. Liu, Z. N. Xu, L. X. Sun, P. Guo, C. F. Zeng, C. Q. Wang and L. X. Zhang, *Chem. Eng. J.*, 2017, **315**, 25–34.
- 53 T. Lin, H. Wang and X. J. A. M. Wang, *Adv. Mater.*, 2005, **17**, 2699–2703.
- 54 M. Kanik, S. Orguc, G. Varnavides, J. Kim, T. Benavides, D. Gonzalez, T. Akintilo, C. C. Tasan, A. P. Chandrakasan, Y. Fink and P. Anikeeva, *Science*, 2019, **365**, 145–150.
- 55 M. J. Tang, W. Wang, Z. L. Li, Z. M. Liu, Z. Y. Guo, H. Y. Tian, Z. Liu, X. J. Ju, R. Xie and L. Y. Chu, *Ind. Eng. Chem. Res.*, 2018, **57**, 9430–9438.
- 56 H. Y. Cheng, J. K. Meng, G. Wu and S. Chen, *Angew. Chem., Int. Ed.*, 2019, **58**, 17465–17473.

- 57 C. H. Choi, H. Yi, S. Hwang, D. A. Weitz and C. S. Lee, *Lab Chip*, 2011, **11**, 1477–1483.
- 58 J. Lölsberg, J. Linkhorst, A. Cinar, A. Jans, A. J. C. Kuehne and M. Wessling, *Lab Chip*, 2018, **18**, 1341–1348.
- 59 J. Bae, J. Lee, Q. Zhou and T. Kim, *Adv. Mater.*, 2019, **31**, e1804953.
- 60 J. Bae, K. Lee, S. Seo, J. G. Park, Q. Zhou and T. Kim, *Nat. Commun.*, 2019, **10**, 1–9.
- 61 M. A. M. Gijs, F. Lacharme and U. Lehmann, *Chem. Rev.*, 2010, **110**, 1518–1563.
- 62 Y. Jun, E. Kang, S. Chae and S.-H. Lee, *Lab Chip*, 2014, **14**, 2145–2160.
- 63 B. B. Patel, M. C. McNamara, L. S. Pesquera-Colom, E. M. Kozik, J. Okuzonu, N. N. Hashemi and D. S. Sakaguchi, *ACS Omega*, 2020, **5**, 7910–7918.
- 64 D. Y. Park, C. H. Mun, E. Kang, D. Y. No, J. Ju and S. H. Lee, *Biofabrication*, 2014, **6**, 024108.
- 65 R. V. Bell, C. C. Parkins, R. A. Young, C. M. Preuss, M. M. Stevens and S. A. F. Bon, *J. Mater. Chem. A*, 2016, **4**, 813–818.
- 66 R. Cheng, F. C. Li, J. H. Zhang, X. J. She, Y. Zhang, K. J. Shao, Y. X. Lin, C. F. Wang and S. Chen, *J. Mater. Chem. C*, 2019, **7**, 4244–4249.
- 67 E. Hofmann, K. Kruger, C. Haynl, T. Scheibel, M. Trebbin and S. Forster, *Lab Chip*, 2018, **18**, 2225–2234.
- 68 D. A. Boyd, A. A. Adams, M. A. Daniele and F. S. Ligler, *J. Visualized Exp.*, 2014, 50958, DOI: 10.3791/50958.
- 69 H. N. He, C. J. Yang, F. Wang, Z. Wei, J. L. Shen, D. Chen, C. H. Fan, H. J. Zhang and K. Liu, *Angew. Chem., Int. Ed.*, 2020, **59**, 4344–4348.
- 70 E. Kang, G. S. Jeong, Y. Y. Choi, K. H. Lee, A. Khademhosseini and S.-H. Lee, *Nat. Mater.*, 2011, **10**, 877–883.
- 71 B. G. Chung, K. H. Lee, A. Khademhosseini and S. H. Lee, *Lab Chip*, 2012, **12**, 45–59.
- 72 T. Sun, X. Li, Q. Shi, H. Wang, Q. Huang and T. Fukuda, *Gels*, 2018, **4**, 38.
- 73 Q. L. Zhao, H. Q. Cui, Y. L. Wang and X. M. Du, *Small*, 2020, **16**, 1903798.
- 74 L. R. Shang, Y. Cheng and Y. J. Zhao, *Chem. Rev.*, 2017, **117**, 7964–8040.
- 75 L. R. Shang, Y. R. Yu, Y. X. Liu, Z. Y. Chen, T. T. Kong and Y. Zhao, *ACS Nano*, 2019, **13**, 2749–2772.
- 76 X. L. Hu, M. W. Tian, T. L. Xu, X. T. Sun, B. Sun, C. C. Sun, X. Q. Liu, X. J. Zhang and L. J. Qu, *ACS Nano*, 2020, **14**, 559–567.
- 77 R. Xie, P. Xu, Y. Liu, L. Li, G. Luo, M. Ding and Q. Liang, *Adv. Mater.*, 2018, **30**, 1705082.
- 78 J. Cai, D. Ye, Y. Wu, L. Fan and H. Yu, *Compos. Commun.*, 2019, **15**, 1–5.
- 79 L. W. Honaker, S. Vats, M. Anyfantakis and J. P. F. Lagerwall, *J. Mater. Chem. C*, 2019, **7**, 11588–11596.
- 80 Y. Cheng, F. Y. Zheng, J. Lu, L. R. Shang, Z. Y. Xie, Y. J. Zhao, Y. P. Chen and Z. Z. Gu, *Adv. Mater.*, 2014, **26**, 5184–5190.
- 81 M. Numata, Y. Takigami, M. Takayama, T. Kozawa and N. Hirose, *Chem. – Eur. J.*, 2012, **18**, 13008–13017.
- 82 J. H. Guo, Y. R. Yu, H. Wang, H. Zhang, X. X. Zhang and Y. J. Zhao, *Small*, 2019, **15**, 1805162.
- 83 W. J. Lan, Y. J. Du, X. Q. Guo, A. X. Liu, S. Jing and S. W. Li, *Ind. Eng. Chem. Res.*, 2018, **57**, 212–219.
- 84 F. Sharifi, Z. H. Bai, R. Montazami and N. Hashemi, *RSC Adv.*, 2016, **6**, 55343–55353.
- 85 H. Yang and M. Guo, *Macromol. Rapid Commun.*, 2019, **40**, 1900111.
- 86 S. Rammensee, U. Slotta, T. Scheibel and A. R. Bausch, *Proc. Natl. Acad. Sci. U. S. A.*, 2008, **105**, 6590–6595.
- 87 Q. F. Peng, H. L. Shao, X. C. Hu and Y. P. Zhang, *Macromol. Mater. Eng.*, 2017, **302**, 1700102.
- 88 A. Rising and J. Johansson, *Nat. Chem. Biol.*, 2015, **11**, 309–315.
- 89 Y. W. Liu, J. Ren and S. J. Ling, *Compos. Commun.*, 2019, **13**, 85–96.
- 90 A. Paul, V. Pisano, A. Polini, M. R. Dokmeci and A. Khademhosseini, *Lab Chip*, 2013, 3989–3992.
- 91 X. Y. Du, Q. Li, G. Wu and S. Chen, *Adv. Mater.*, 2019, **31**, 1903733.
- 92 W. Jeong, J. Kim, S. Kim, S. Lee, G. Mensing and D. J. Beebe, *Lab Chip*, 2004, **4**, 576–580.
- 93 S. Shin, J. Y. Park, J. Y. Lee, H. Park, Y. D. Park, K. B. Lee, C. M. Whang and S. H. Lee, *Langmuir*, 2007, **23**, 9104–9108.
- 94 X. L. Zhang, L. L. Wang, L. Weng and B. Y. Deng, *J. Appl. Polym. Sci.*, 2020, **137**, 48571.
- 95 W. W. Lin, Y. S. Ni and J. Pang, *Int. J. Biol. Macromol.*, 2020, **149**, 853–860.
- 96 L.-L. Xu, C.-F. Wang and S. Chen, *Angew. Chem., Int. Ed.*, 2014, **53**, 3988–3992.
- 97 J. Kim, J. W. Hong, D. P. Kim, J. H. Shin and I. Park, *Lab Chip*, 2012, **12**, 2914–2921.
- 98 Y. Srivastava, M. Marquez and T. Thorsen, *J. Appl. Polym. Sci.*, 2007, **106**, 3171–3178.
- 99 B. Khalid, X. P. Bai, H. H. Wei, Y. Huang, H. Wu and Y. Cui, *Nano Lett.*, 2017, **17**, 1140–1148.
- 100 R. Vasireddi, J. Kruse, M. Vakili, S. Kulkarni, T. F. Keller, D. C. F. Monteiro and M. Trebbin, *Sci. Rep.*, 2019, **9**, 1–10.
- 101 H. Cheng, J. Meng, G. Wu and S. Chen, *Angew. Chem., Int. Ed.*, 2019, **58**, 17465–17473.
- 102 J. Kameoka and H. G. Craighead, *Appl. Phys. Lett.*, 2003, **83**, 371–373.
- 103 F. Zhang, W. Li, Z. Xu, M. Ye, W. Guo, H. Xu and X. Liu, *RSC Adv.*, 2017, **7**, 52988–52994.
- 104 Q. Liu, Z. Xu, W. Qiu, C. Hou, Y. Wang, P. Yao, R. Yu, W. Guo and X. Y. Liu, *RSC Adv.*, 2018, **8**, 18690–18697.
- 105 H. Onoe, T. Okitsu, A. Itou, M. Kato-Negishi, R. Gojo, D. Kiriya, K. Sato, S. Miura, S. Iwanaga, K. Kuribayashi-Shigetomi, Y. T. Matsunaga, Y. Shimoyama and S. Takeuchi, *Nat. Mater.*, 2013, **12**, 584–590.
- 106 K. H. Lee, S. J. Shin, Y. Park and S.-H. Lee, *Small*, 2009, **5**, 1264–1268.
- 107 M. A. Daniele, D. A. Boyd, A. A. Adams and F. S. Ligler, *Adv. Healthcare Mater.*, 2015, **4**, 11–28.
- 108 J.-H. Jung, C.-H. Choi, S. Chung, Y.-M. Chung and C.-S. Lee, *Lab Chip*, 2009, **9**, 2596–2602.

- 109 E. Kang, Y. Y. Choi, S. K. Chae, J. H. Moon, J. Y. Chang and S. H. Lee, *Adv. Mater.*, 2012, **24**, 4271–4277.
- 110 Y. Yu, W. B. Wei, Y. Q. Wang, C. Xu, Y. Q. Guo and J. H. Qin, *Adv. Mater.*, 2016, **28**, 6649–6655.
- 111 X. L. Zhang, L. Weng, Q. S. Liu, D. W. Li and B. Y. Deng, *R. Soc. Open Sci.*, 2019, **6**, 181928.
- 112 Y. M. Zheng, H. Bai, Z. B. Huang, X. L. Tian, F. Q. Nie, Y. Zhao, J. Zhai and L. Jiang, *Nature*, 2010, **463**, 640–643.
- 113 Y. H. Cai, L. H. Geng, S. Chen, S. Shi, B. S. Hsiao and X. F. Peng, *ACS Appl. Mater. Interfaces*, 2020, **12**, 32090–32098.
- 114 S. Y. Li, Y. J. Hang, Z. Z. Ding, Q. Lu, G. Z. Lu, H. Chen and D. L. Kaplan, *ACS Biomater. Sci. Eng.*, 2020, **6**, 2847–2854.
- 115 X. L. Hu, M. W. Tian, B. Sun, L. J. Qu, S. F. Zhu and X. S. Zhang, *Mater. Lett.*, 2018, **230**, 148–151.
- 116 J. Luo, L. L. Zhang, Q. F. Peng, M. J. Sun, Y. P. Zhang, H. L. Shao and X. C. Hu, *Int. J. Biol. Macromol.*, 2014, **66**, 319–324.
- 117 W. Qiu, A. Patil, F. Hu and X. Y. Liu, *Small*, 2019, **15**, 1903948.
- 118 A. Kazemzadeh, P. Ganesan, F. Ibrahim, M. M. Aeinehvand, L. Kulinsky and M. J. Madou, *Sens. Actuators, B*, 2014, **204**, 149–158.
- 119 R. Wu, L. Ma, S. Liu, A. B. Patil, C. Hou, Y. Zhang, W. Zhang, R. Yu, W. Yu, W. Guo and X. Y. Liu, *Mater. Today Phys.*, 2020, **15**, 100243.
- 120 L. Ma, R. Wu, S. Liu, A. Patil, H. Gong, J. Yi, F. Sheng, Y. Zhang, J. Wang, J. Wang, W. Guo and Z. L. Wang, *Adv. Mater.*, 2020, 2003897.
- 121 A. Maziz, A. Concas, A. Khaldi, J. Stalhand, N. K. Persson and E. W. H. Jager, *Sci. Adv.*, 2017, **3**, e1600327.
- 122 K. Jost, D. Stenger, C. R. Perez, J. K. McDonough, K. Lian, Y. Gogotsi and G. Dion, *Energy Environ. Sci.*, 2013, **6**, 2698–2705.
- 123 Z. Tang and R. Postle, *Compos. Struct.*, 2000, **49**, 451–459.
- 124 X. H. He, W. Wang, Y. M. Liu, M. Y. Jiang, F. Wu, K. Deng, Z. Liu, X. J. Ju, R. Xie and L. Y. Chu, *ACS Appl. Mater. Interfaces*, 2015, **7**, 17471–17481.
- 125 D. Park, J. Park, H. Jang, J. Cheng, S. Hyun Kim and S. H. Lee, *Biofabrication*, 2017, **9**, 025026.
- 126 K. Ma, X.-Y. Du, Y.-W. Zhang and S. Chen, *J. Mater. Chem. C*, 2017, **5**, 9398–9404.
- 127 Y. Zhang, C. F. Wang, L. Chen, S. Chen and A. J. Ryan, *Adv. Funct. Mater.*, 2015, **25**, 7253–7262.
- 128 X. Lu, Y. Hu, J. Z. Guo, C. F. Wang and S. Chen, *Adv. Sci.*, 2019, **6**, 1901694.
- 129 G. S. Jeong and S.-H. Lee, *Tissue Eng. Regener. Med.*, 2014, **11**, 291–296.
- 130 X. Shi, S. Ostrovidov, Y. Zhao, X. Liang, M. Kasuya, K. Kurihara, K. Nakajima, H. Bae, H. Wu and A. Khademhosseini, *Adv. Funct. Mater.*, 2015, **25**, 2250–2259.
- 131 B. R. Lee, K. H. Lee, E. Kang, D.-S. Kim and S.-H. Lee, *Biomicrofluidics*, 2011, **5**, 022208.
- 132 C. M. Hwang, A. Khademhosseini, Y. Park, K. Sun and S. H. Lee, *Langmuir*, 2008, **24**, 6845–6851.
- 133 C. Tian, Q. Tu, W. M. Liu and J. Y. Wang, *TrAC, Trends Anal. Chem.*, 2019, **117**, 146–156.
- 134 T. Sun, Q. Huang, Q. Shi, H. P. Wang, X. M. Liu, M. Seki, M. Nakajima and T. Fukuda, *Microfluid. Nanofluid.*, 2015, **19**, 1169–1180.
- 135 J. Cheng, D. Park, Y. Jun, J. Lee, J. Hyun and S. H. Lee, *Lab Chip*, 2016, **16**, 2654–2661.
- 136 S. Y. Ahn, C. H. Mun and S. H. Lee, *RSC Adv.*, 2015, **5**, 15172–15181.
- 137 Y. S. Ni, W. M. Lin, R. J. Mu, C. H. Wu, L. Wang, D. Wu, S. Chen and J. Pang, *RSC Adv.*, 2018, **8**, 26432–26439.
- 138 H. Zhang, G. P. Chen, Y. R. Yu, J. H. Guo, Q. Tan and Y. N. Zhao, *Adv. Sci.*, 2020, **7**, 2000789.
- 139 X. J. Wu, Y. J. Xu, Y. Hu, G. Wu, H. Y. Cheng, Q. Yu, K. Zhang, W. Chen and S. Chen, *Nat. Commun.*, 2018, **9**, 1–11.
- 140 T. Xu, X. T. Ding, Y. Liang, Y. Zhao, N. Chen and L. T. Qu, *Nanoscale*, 2016, **8**, 12113–12117.